

## Article

# Thermal Stability Calculation and Experimental Investigation of Common Binary Chloride Molten Salts Applied in Concentrating Solar Power Plants

Jingyu Zhong<sup>1</sup>, Jing Ding<sup>1,\*</sup>, Jianfeng Lu<sup>1</sup> , Xiaolan Wei<sup>2</sup> and Weilong Wang<sup>1,\*</sup>

<sup>1</sup> School of Materials Science and Engineering, Sun Yat-sen University, Guangzhou 510006, China; zhongjy35@mail2.sysu.edu.cn (J.Z.); lujfeng@mail.sysu.edu.cn (J.L.)

<sup>2</sup> School of Chemistry and Chemical Engineering, South China University of Technology, Guangzhou 510640, China; xlwei@scut.edu.cn

\* Correspondence: dingjing@mail.sysu.edu.cn (J.D.); wwlong@mail.sysu.edu.cn (W.W.)

**Abstract:** A computational study on thermal stability was conducted the first time, combining the modified quasi-chemical model, the Antoine equation, and the adiabatic flash evaporation calculation principle to design a method to calculate the system pressure-temperature (P-T) phase diagram of binary chloride molten salts. The evaporation temperature of the molten salt obtained by analyzing the P-T phase diagram of the eutectic molten salt clearly defined the upper limit of the optimal operating temperature of the mixed molten salt. The results indicated that the upper-temperature limits of NaCl-KCl, NaCl-CaCl<sub>2</sub>, KCl-CaCl<sub>2</sub>, NaCl-MgCl<sub>2</sub>, and KCl-MgCl<sub>2</sub> are determined to be 1141 K, 1151 K, 1176 K, 1086 K, and 1068 K. The maximum working temperature was measured experimentally using a thermogravimetric analysis (TGA), and the relative error between the calculation and experiment was calculated. The maximum error between the calculated and experimental values of the maximum operating temperature was 6.02%, while the minimum was 1.29%, demonstrating the method's high accuracy. Combined with the lowest eutectic temperature and the upper-temperature limits of binary chloride molten salts, the stable operating temperature ranges of NaCl-KCl, NaCl-CaCl<sub>2</sub>, KCl-CaCl<sub>2</sub>, NaCl-MgCl<sub>2</sub>, and KCl-MgCl<sub>2</sub> are 891~1141 K, 750~1151 K, 874~1176 K, 732~1086 K, and 696~1086 K.

**Keywords:** thermal stability calculation; upper-temperature limit; P-T phase diagram; modified quasi-chemical model; adiabatic flash calculation; binary chloride molten salts



**Citation:** Zhong, J.; Ding, J.; Lu, J.; Wei, X.; Wang, W. Thermal Stability Calculation and Experimental Investigation of Common Binary Chloride Molten Salts Applied in Concentrating Solar Power Plants. *Energies* **2022**, *15*, 2516. <https://doi.org/10.3390/en15072516>

Academic Editors: Wei-Hsin Chen and Lyes Bennamoun

Received: 8 February 2022

Accepted: 23 March 2022

Published: 29 March 2022

**Publisher's Note:** MDPI stays neutral with regard to jurisdictional claims in published maps and institutional affiliations.



**Copyright:** © 2022 by the authors. Licensee MDPI, Basel, Switzerland. This article is an open access article distributed under the terms and conditions of the Creative Commons Attribution (CC BY) license (<https://creativecommons.org/licenses/by/4.0/>).

## 1. Introduction

Human beings have been struggling with global warming exacerbating in the aftermath of increasing climate change and huge energy demand issues. Renewable clean energy sources are being developed to reduce the dominance of traditional fossil energy in global energy consumption [1,2]. For example, the scientific community has proposed a cost-effective thermal energy storage (TES) strategy to be combined with concentrated solar power (CSP) plants to ensure the continuity of electricity supply [3–5]. After concentrating the sun's rays by mirrors, solar energy can be stored as thermal energy by the TES system for later use [3,6]. Among TES materials, it is possible for molten salts to meet the high-temperature use requirements of the CSP plant and the goal of TES, owing to their advantages of high heat storage density and efficiency, wide operating temperature range and low economic cost [7,8]. In commercial solar thermal power generation systems, Solar Salt (NaNO<sub>3</sub>-KNO<sub>3</sub>, 60-40 wt.%) and Hitec Salt (NaNO<sub>3</sub>-KNO<sub>3</sub>-NaNO<sub>2</sub>, 7-53-40 wt.%) are two of the most extensive and mature molten salts used as heat transfer and storage media [9–11]. However, nitrates used in CSP plants operate only below 773 K, which is severely limited due to poor thermal stability, which causes nitrates to decompose easily at high temperatures [12–14]. Chloride molten salts have emerged as potential candidates for the next generation of CSP in recent years. Because of their wide working temperature

range and excellent high-temperature stability, chloride molten salts have been found to be suitable for many advanced high-temperature power cycles.

Furthermore, chloride molten salts have been temporarily limited in commercial applications due to the lack of data on thermophysical properties at high temperatures even near the boiling zone, although they meet the heating temperature requirements of high-temperature thermal utilization [15]. The determination of the maximum working temperature of chloride molten salts as future work was strongly suggested in the latest review article [16]. Currently, researchers frequently employ the thermogravimetric analysis (TGA) technique to assess the thermal stability of a molten salt [17–19]. The maximum working temperature of nitrate molten salts is limited by thermal decomposition at high temperatures and is frequently determined by the temperature at which 3 wt.% mass loss occurs [17–19]. Experimental research on the maximum operating temperature of chloride molten salts has also been conducted by many researchers. A substantial mass loss (~1 wt.%) in the 100–200 °C range owing to the vaporization of a minor amount of water and other impurities was reported by conducting 10 separate TGA measurements, each with fresh salts [20]. Since all 10 tests indicated that the mass loss is small enough to be inappreciable in the 200–700 °C range for MgCl<sub>2</sub>-KCl (32–68 mol.%) molten salt, there was a suggestion that the traditional TGA 3 wt.% mass loss method is inapplicable for chloride molten salts, which needs to be improved with other factors. It is demonstrated that the mass loss of chlorides is not caused by thermal decomposition as it is for nitrates, but rather by salt or water vaporization and salt impurity reactions, as investigated using the DSC equipment, TGA technique, X-ray Diffraction (XRD), and Mass Spectrometry (MS) [21,22]. Mass loss owing to the chemical decomposition of molten salt or the evaporation caused by high vapor pressure was distinguished by measuring the mass loss of chloride molten salts in three different atmospheres with DSC-TGA equipment [23]. If corrosion is not taken into account, the maximum working temperature of chloride molten salts was proposed in the above work to be determined by the salt vapor pressure and the gas atmosphere.

In summary, the maximum upper operating temperature of chloride molten salt is not limited by thermal decomposition like nitrate, but by other factors, such as salt vapor pressure or corrosivity regarding salt impurities [16]. It takes a long time to investigate the maximum operating temperatures of chloride molten salts using experiments with a large workload and a high level of uncertainty. Nonetheless, at the time of writing, the upper limit of the operation temperature of molten salts had not yet been discovered through modeling and computation research. In the past, a lot of experience has been accumulated using phase diagram calculation methods to predict the composition and lowest eutectic point of unknown multicomponent molten salt materials, which determined the lower limit of the optimal working temperature of molten salts in service conditions. Using the modified quasi-chemical model through the FactSage software, binary and ternary phase diagrams of some alkali metal and rare earth metal chlorides were optimized, which were then combined with experimental data to determine the best calculation model parameters [24–26]. The phase diagrams of the fluoride and chloride molten salt system with and without compound formation were calculated adopting the Regular Solution Model, and the influence the interaction coefficients of the binary boundary system will have on the isotherm of the ternary system was specifically analyzed [27]. It would be a significant breakthrough if we could calculate the highest working temperature of chloride molten salts using phase diagram computation, just as we can calculate the lowest eutectic point using the solid-liquid phase diagram. The computational method has the advantage of increasing the efficiency of the study on the maximum working temperature of chloride molten salts and reducing the experimental workload by reporting a predicted value in advance.

To implement molten salt materials in CSP, low vapor pressure is favorable, as vapor pressure is a thermophysical parameter required to fully characterize molten salts [17]. Taking chloride molten salt evaporation as a consideration, this work studied the evaporation temperature of five binary chloride molten salts. Based on the analysis of the vapor-liquid

phase equilibrium thermodynamic model of common binary chloride molten salt systems, this paper established a computation method of the P-T phase diagram of binary molten chlorides expressed in equal molar mass proportions. The P-T phase diagrams of five binary chloride salts—NaCl-KCl, NaCl-CaCl<sub>2</sub>, KCl-CaCl<sub>2</sub>, NaCl-MgCl<sub>2</sub>, and KCl-MgCl<sub>2</sub>—were calculated using the adiabatic flash evaporation calculation principle. For the first time, the maximum working temperature of the binary chloride salts was determined through computational calculation. The calculation results were relatively accurate and verified by TGA, proving the feasibility of the method.

## 2. Materials and Methods

Considering the vapor pressure of chloride molten salt, the water in the salt or the salt itself may evaporate at high temperatures, causing a mass loss under service. At this point, the molten chloride system transitions from liquid to vapor, and vapor liquid equilibrium calculations can be used to investigate the evaporation of chloride molten salts. For the binary chloride molten salt with the lowest eutectic point and the corresponding optimal components ratio and the relationship between system pressure and temperature can be obtained by calculating the vapor liquid phase diagram of the salt under that ratio. By analyzing the evaporation temperature obtained from the P-T phase diagram of the eutectic molten salt, the upper optimal working temperature of molten chlorides can be clearly defined. The temperature point at one atmospheric pressure on the pressure temperature curve is the critical point of the vapor liquid two phases, where the temperature is the molten salt's evaporation temperature [28]. In the field of organics and alloys, the P-T phase diagram exploration is more common. For instance, the P-T phase diagram of the ferroelectric clathrate bithiourea pyridine bromide was constructed through dielectric spectroscopy, neutron and X-ray diffraction and nuclear magnetic resonance, and the effects of temperature and pressure on their physical properties were studied in the meantime [29]. In another article, the P-T-x-y phase diagram of the Cd-Zn-Te system was constructed to discuss the character of the sublimation of the Cd<sub>1-x</sub>Zn<sub>x</sub>Te (CZT) solid solution [30].

Before calculating, based on necessary considerations, the four following assumptions were made: (1) heat exchange could not occur with the outside world in the chloride molten salt system; (2) the system is under high temperature and normal pressure when in equilibrium; (3) ideal gas state equation is followed; and (4) the liquid phase is treated as a nonideal solution.

### 2.1. Vapor Liquid Phase Equilibrium Thermodynamic Theory

The exchange of energy and matter occurs when the two vapor liquid phases are in contact with each other. When the properties of each phase no longer change, the system is said to be in vapor liquid equilibrium. The fugacity of each component in the vapor and liquid phases is equal at this point, as shown in Equation (1) [31].

$$\hat{f}_i^V(T, P, y_i) = \hat{f}_i^L(T, P, x_i) \quad (1)$$

where  $\hat{f}_i^V$  and  $\hat{f}_i^L$  represent the fugacity of component  $i$ , respectively, in the vapor and liquid phases.  $x_i$  is the mole fraction of component  $i$  in the liquid phase, while  $y_i$  is the mole fraction of component  $i$  in the vapor phase; the system pressure is represented by  $P$ .

Since the system is under normal pressure without the heat exchange assumed in this work, the activity coefficient method was used for the vapor liquid phase equilibrium calculation. The fugacity coefficient and the activity coefficient are used to express the fugacity of the vapor phase component and the liquid phase component, respectively.

$$\hat{f}_i^V(T, P, y_i) = \hat{\Phi}_i^V P y_i \quad (2)$$

$$\hat{f}_i^L(T, P, x_i) = r_i x_i p_i^s \Phi_i^* \exp \left[ V_i^l (P - p_i^s) / RT \right] \quad (3)$$

where  $\hat{\Phi}_i^v$  represents the fugacity coefficient of component  $i$  in the vapor phase, and  $\Phi_i^*$  represents the fugacity coefficient of component  $i$  in the liquid phase. The activity coefficient of component  $i$  in the liquid phase, the saturated vapor pressure of component  $i$  at temperature  $T$  and the molar volume of pure component  $i$  can be expressed as  $r_i$ ,  $p_i^s$ ,  $V_i^l$  correspondingly, while  $R$  represents the thermodynamic constant.

Based on Equations (1) and (2) [31], and (3) [31], the following Equation (4) [31] can be obtained:

$$\hat{\Phi}_i^v P y_i = \Phi_i^* p_i^s r_i x_i \exp \left[ V_i^l (P - p_i^s) / RT \right] \quad (4)$$

## 2.2. Adiabatic Flash Calculation Theory

In this work, the adiabatic flash calculation theory was introduced to calculate the pressure temperature (P-T) phase diagram, considering that molten chloride salt with high vapor pressure will evaporate at high temperature. To obtain the P-T phase diagram of molten chlorides, the activity coefficient, obtained using the modified quasi-chemical model, and the saturated vapor pressure, calculated using the Antoine equation, were substituted into the adiabatic flash calculation. The activity coefficient and the vapor pressure were used as parameters in the adiabatic flash evaporation calculation process, and ultimately served for the calculation of the relationship of system pressure and temperature.

For chloride molten salt system, there are three basic phase characteristics in its gas and liquid two-phases: (a) bubble point state; (b) dew point state; (c) flash equilibrium state, as shown in Figure 1. The bubble point is the point at which the liquid phase begins to bubble and boil, and the dew point is the point at which the gas phase begins to condense into dew-like droplets.

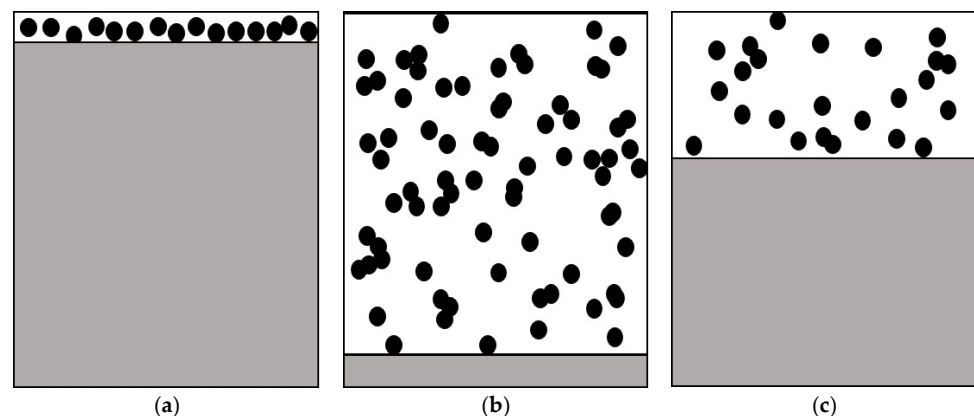


**Figure 1.** Basic phase characteristics of chloride molten salt system: (a) bubble point state; (b) dew point state; and (c) flash equilibrium state.

### 2.2.1. Adiabatic Flash Calculation

Flash evaporation is a single equilibrium stage distillation process. The vapor phase is enriched in volatile components, while the liquid phase is enriched in heavy components. The basic equations of flash calculation are the mass balance equation, phase balance equation, and energy balance equation, as shown below in Equations (5)–(7) [32],

$$z_i = y_i v + x_i (1 - v) \quad i = 1, 2, \dots, n \quad (5)$$

$$K_i = r_i \Phi_i^s p_i^s (PF)_i / \left( \hat{\Phi}_i^v P \right) \quad i = 1, 2, \dots, n \quad (6)$$

$$H_F + Q/F = v H_v + (1 - v) H_l \quad (7)$$

where  $z_i$  represents the total composition before operation of component  $i$ , while  $v$  is the vaporization rate.  $K_i$  is the vapor-liquid equilibrium ratio of component  $i$ , which is defined as the ratio of the molar fractions of the components in the two vapor liquid phases, as shown in Equation (8) [32].  $\Phi_i^s$  represents the saturated liquid fugacity coefficient of component  $i$ , respectively. The Poynting factor of component  $i$  is abbreviated as  $(PF)_i$ .  $H_F$ ,  $H_v$ , and  $H_l$  are the molar enthalpies of the mixture, vapor, and liquid phases, respectively, while  $Q$  is the endothermic heat of the process.  $F$  is the total amount of the system, which is a known quantity, and hence, can be regarded as a constant.

$$K_i = y_i/x_i \tag{8}$$

Combining Equations (5) and (8), the two formulas for calculating the vapor phase composition and the liquid phase composition can be obtained.

$$y_i = z_i K_i / [1 + v(K_i - 1)] \quad i = 1, 2, \dots, n \tag{9}$$

$$x_i = z_i / [1 + v(K_i - 1)] \quad i = 1, 2, \dots, n \tag{10}$$

Since the system is under high temperature and normal pressure when in equilibrium, the vapor phase can be treated as an ideal gas mixture,  $\hat{\Phi}_i^v = 1$  and  $\Phi_i^s(PF)_i$  can be approximated as 1. As a result, Equation (6) can be rewritten as follows:

$$K_i = r_i p_i^s / P \quad i = 1, 2, \dots, n \tag{11}$$

Barometric pressure 760 mmHg could be taken as the initial value of system pressure, which afterwards calculated by the following Equation (12) [32]. Due to  $\sum_i y_i = 1$ , combing Equations (8) and (11) and summing over all samples gives the following formation:

$$P = x_i r_i p_i^s + x_j r_j p_j^s \tag{12}$$

The activity coefficient  $r_i$  can be calculated by the modified quasi-chemical model, which will be described later in detail. As for the saturated vapor pressure  $p_i^s$ , it is an indispensable parameter in the adiabatic flash evaporation calculation process, as shown in Figures 2–5. In the calculation flow, as the loop parameter  $T$  is iteratively calculated, the corresponding  $p_i^s$  is constantly recalculated.

The saturated vapor pressure  $p_i^s$  of the pure component  $i$  can be calculated by applying the Antoine equation [32], which can provide high-accuracy data,

$$\lg p_i^s = -B_i/T + A_i \tag{13}$$

or

$$\lg p_i^s = -B_i/T - C_i/T + A_i \tag{14}$$

where  $A_i$ ,  $B_i$ , and  $C_i$  are Antoine constants of component  $i$ , which are published in the general physical property data manual.

Considering the adiabatic conditions of the system,  $Q = 0$ , and the energy balance Equation (7) can be written as follows:

$$H_F = vH_v + (1 - v)H_l \tag{15}$$

where  $H_v$ , and  $H_l$  can be calculated as Equations (16) and (17) [32]:

$$H_l = (1 - v) \sum x_i C_{pl} T \tag{16}$$

and

$$H_v = v \sum y_i C_{pv} T \tag{17}$$

where  $Cpl_i$  and  $Cpv_i$  are the liquid specific heat capacity and vapor specific heat capacity of component  $i$ , respectively.

Knowing that the temperature  $T$  is an unknown quantity, its initial value should be assumed between the precalculated bubble point and dew point temperature, and then the initial value of  $T$  should be iteratively calculated and adjusted until Equation (15) is satisfied. In addition, the temperature value  $T$  is not sensitive to the vaporization rate  $v$  for mixtures with a narrow boiling range. For calculation, in consequence, it is more appropriate to use  $T$  as the internal iteration variable and  $v$  as the external iteration variable. Accordingly, the initial value of  $v$  is calculated by interpolating the precalculated bubble point and dew point temperature as in Equation (18) [32].

$$v = (T_b - T)/(T_b - T_d) \tag{18}$$

For the narrow boiling range system, as shown in Figure 2, the adiabatic flash evaporation calculation process is a sequential algorithm, wherein the inner cycle parameter is the temperature  $T$  and the outer cycle parameter is the vaporization rate  $v$ . Both  $T$  and  $v$  are solved by the Newton iteration method, and the convergence accuracies for both are 0.001. The objective function and the Newton method iteration equation of  $T$  and  $v$  are shown below [32].

$$HT = H_F - H_0 \tag{19}$$

$$T = T - HT/dHT \tag{20}$$

$$Fv = \sum z_i(K_i - 1)/[1 + v(K_i - 1)] \tag{21}$$

$$v = v - Fv/dFv \tag{22}$$

$H_0$ ,  $HT$ , and  $dHT$  are the molar enthalpy of the system before operation, the enthalpy change, and its derivative value during the working process of the system, respectively.

$$H_0 = \sum z_i Cpl_i T \tag{23}$$

$$dHT = v \cdot Cpv + (1 - v) \cdot Cpl \tag{24}$$

Since the sum of the vapor phase mole fraction and the liquid phase mole fraction are both 1, the objective function of  $v$  can be obtained as  $Fv$ , and the derivative of  $Fv$  is  $dFv$ .

$$dFv = -\sum z_i \{(K_i - 1)/[1 + v(K_i - 1)]\}^2 \tag{25}$$

The wide boiling range system in which the outer cycle parameter is  $T$  and the inner cycle parameter is  $v$ , is opposite to the narrow boiling range system (Figure 3).

### 2.2.2. Bubble Point and Dew Point Temperature Calculation

The iterative calculation method is commonly used to calculate the bubble point and dew point temperature, and the initial temperature value must be input at the start of the iterative algorithm. Because the system pressure is not significantly different from the saturated vapor pressure of the pure component, it can be used as a replacement in the first trial calculation. Moreover, the saturated temperature of the pure component can be inversely calculated by the Antoine equation as follows:

$$T_i^s = -B_i / (\lg P - A_i) \tag{26}$$

where  $T_i^s$  is the saturated temperature of the component  $i$ . In the case of Equation (14), however,  $T_i^s$  needs to be solved by the dichotomy numerical calculation method.

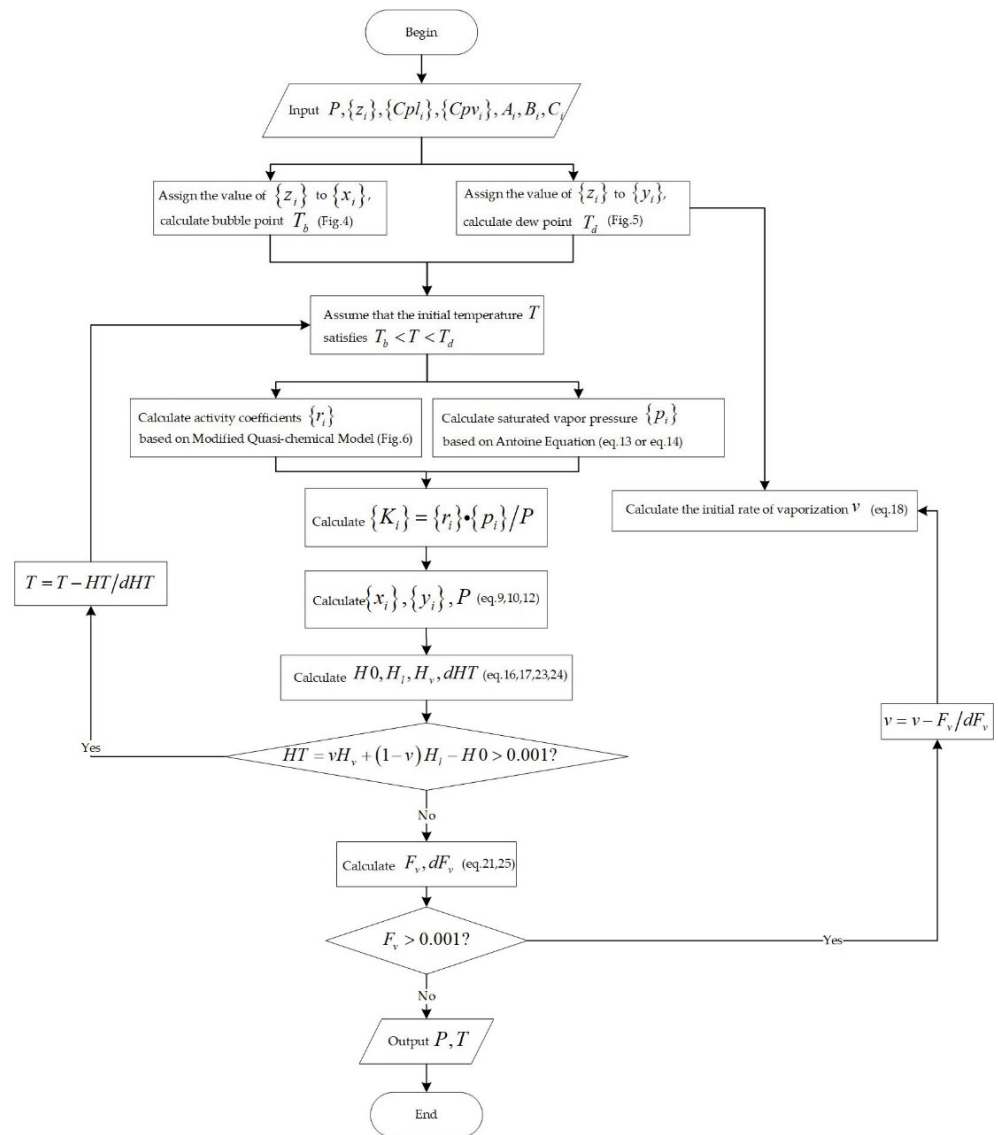


**Figure 2.** Flowchart for the calculation of adiabatic flash for narrow boiling range mixtures.

The initial temperature value can be calculated by linearly adding up the saturation temperature of each component. For the bubble point temperature calculation, the initial value of  $T$  is calculated as follows [32]:

$$T_0 = \sum_i x_i T_i^s \quad (27)$$

After calculating  $r_i$  using the modified quasi-chemical model and  $p_i$  using the Antoine equation,  $y_i$  is calculated by combining Equations (8), (9) and (11).

The vapor pressure ratio [32] is introduced to calculate the saturated vapor pressure of component  $j$ ,

$$p_{jb} = P \sum_i (y_i / r_i) (p_j / p_i) \quad (28)$$

Once  $p_{jb}$  is determined, the Antoine equation can be used to inversely calculate the system temperature, as shown in Figure 4. After iteration, finally, the bubble point temperature  $T_b$  is calculated.

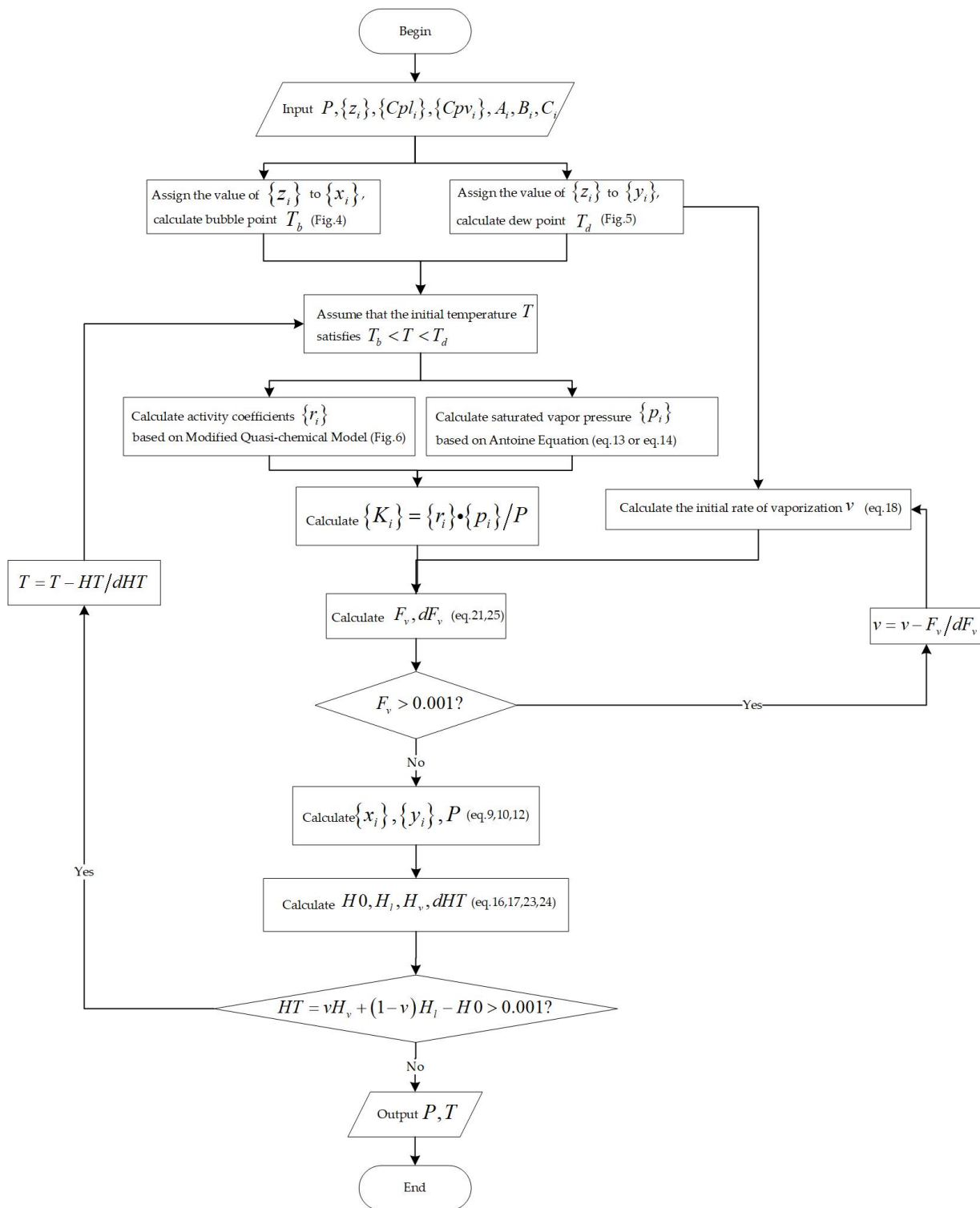


**Figure 3.** Flowchart for the calculation of adiabatic flash for wide boiling range mixtures.

Similarly, for the dew point temperature calculation, the initial value of  $T$  is calculated as follows [32]:

$$T_0 = \sum_i y_i T_i^s \quad (29)$$

Figure 5 illustrates the flow chart of the dew point temperature calculation. After calculating  $p_i$  using the Antoine equation,  $x_i$  is calculated by combining Equations (8), (10) and (11).  $T_d$  is then calculated according to Equation (27). Subsequently,  $p_{jd}$  is calculated accord-

ing to the following equation [32] after obtaining  $r_{id}$  according to the modified quasi-chemical model.

$$p_{jd} = P / \left[ \sum_i x_i r_{id} (p_i / p_j) \right]. \tag{30}$$

Further, we calculate  $T_d$  and  $p_{id}$  in turn, using the Antoine equation with  $p_{id}$ , and obtain  $y_{id}$  according to Equations (8), (9) and (11). After iteration, the dew point temperature  $T_d$  is calculated.

### 2.2.3. Modified Quasi-Chemical Model

Because the liquid phase of the molten salt system is treated as a nonideal solution in the assumptions made in this article, the modified quasi-chemical model [33–35] was applied to calculate the solution’s activity coefficient. Taking the binary system as an example, the quasi-chemical theory only considers the interactions between the nearest neighbor bonds. It is believed that there are three coordination forms when component 1 and component 2 are mixing, as shown below in Equation (31) [33].



In the equation above, the coordination form  $[1 - 2]$  is derived from the coordination form of  $[1 - 1]$  and  $[2 - 2]$ . Hence, the total excess Gibbs free energy ( $\Delta G^E$ ) is calculated as follows [34]:

$$\Delta G^E = RTZ(b_1x_1 + b_2x_2)\{Y_1 \ln(\xi - 1 + 2Y_1) - Y_1 \ln[Y_1(1 + \xi)] + Y_2 \ln(\xi - 1 + 2Y_2) - Y_2 \ln[Y_2(1 + \xi)]\} / 2 \tag{32}$$

$$\xi = \sqrt{1 + 4x_1x_2\{\exp[2(\omega - T\eta)/(zRT)] - 1\}} \tag{33}$$

where  $R$  and  $z$  represent the thermodynamic constant and the coordination number in quasi-lattice model, respectively.

The modified quasi-chemical model pays attention to the molar enthalpy change  $\omega$  and non-configurational entropy change  $\eta$  of the components to express the model more clearly. On this basis, the equivalent fraction  $Y_i$  is introduced [34].

$$\omega = \omega_0 + \omega_1Y_2 + \omega_2Y_2^2 + \omega_3Y_2^3 + \dots \tag{34}$$

$$\eta = \eta_0 + \eta_1Y_2 + \eta_2Y_2^2 + \eta_3Y_2^3 + \dots \tag{35}$$

$$Y_1 = b_1x_1 / (b_1x_1 + b_2x_2) \tag{36}$$

$$Y_2 = b_2x_2 / (b_1x_1 + b_2x_2) \tag{37}$$

The selection of appropriate  $b_1$  and  $b_2$  would maximize components order of the system, under which  $Y_1 = Y_2 = \frac{1}{2}$  [34]. In the meanwhile,  $b_1, b_2$  can be calculated as follows [34], where  $\epsilon$  related to the composition of the system with maximum order.

$$b_2z = -[\ln \epsilon + (1 - \epsilon) \ln(1 - \epsilon) / \epsilon] / \ln 2 \tag{38}$$

$$b_1 = b_2\epsilon / (1 - \epsilon) \tag{39}$$

$$\epsilon = b_1 / (b_1 + b_2) \tag{40}$$

The relationship between the molar excess free energy and partial molar excess free energy is as follows [33]:

$$\overline{G}_i^E = G^E + (1 - x_i) \left( \partial G^E / \partial x_i \right)_{T,P} \tag{41}$$

Incorporating Equations (32)–(37) and (41), the partial molar excess free energy of components 1 and 2 can be calculated [35].

$$\overline{G}_1^E = b_1 RTz \ln\{(\xi - 1 + 2Y_1)/[Y_1(1 + \xi)]\}/2 - 2b_1 Y_1 Y_2^2 [\partial(\omega - T\eta)/\partial Y_2]/(1 + \xi) \quad (42)$$

$$\overline{G}_2^E = b_2 RTz \ln\{(\xi - 1 + 2Y_2)/[Y_2(1 + \xi)]\}/2 + 2b_2 Y_2 Y_1^2 [\partial(\omega - T\eta)/\partial Y_2]/(1 + \xi) \quad (43)$$

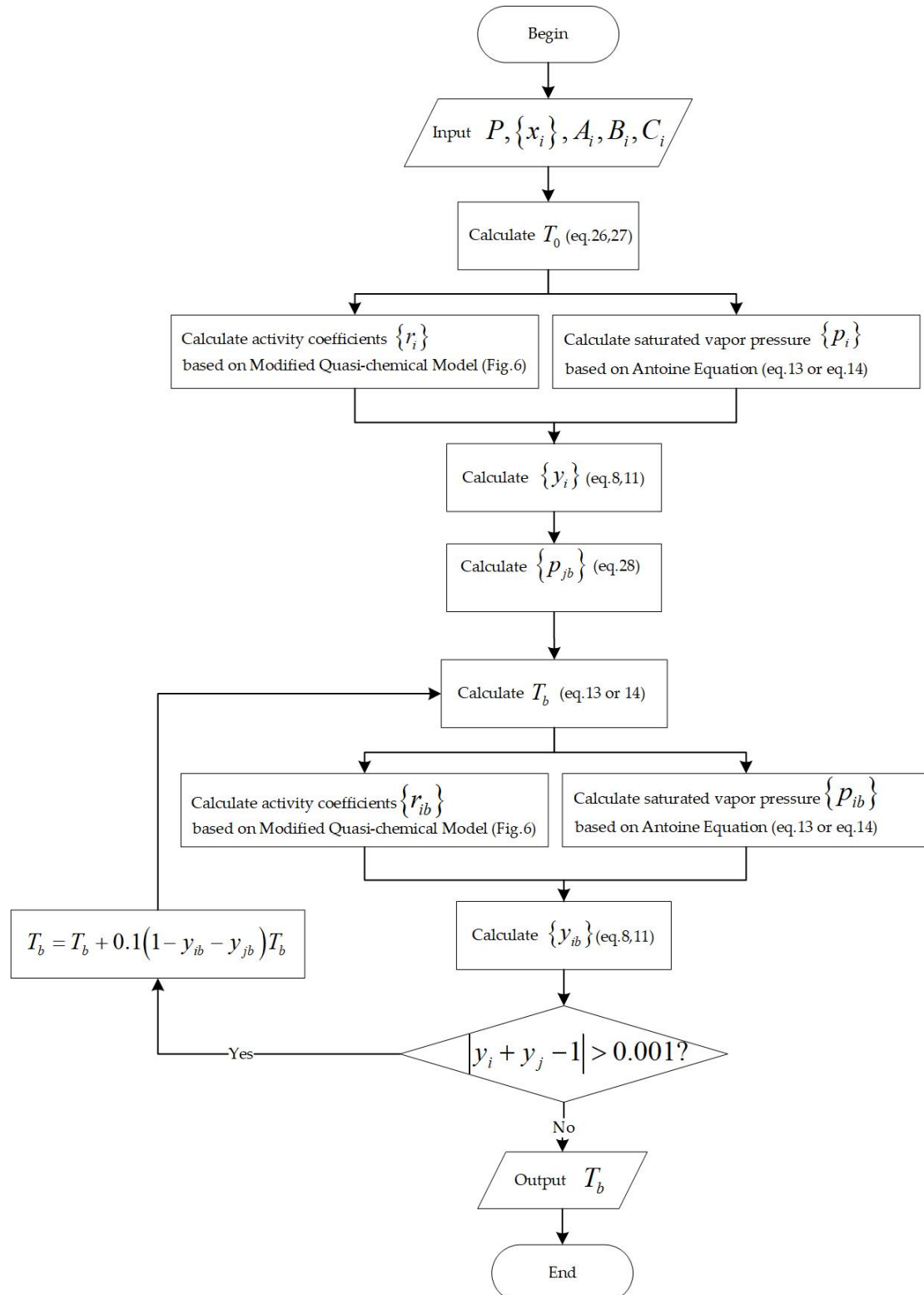


Figure 4. Flowchart for the calculation of bubble point temperature.

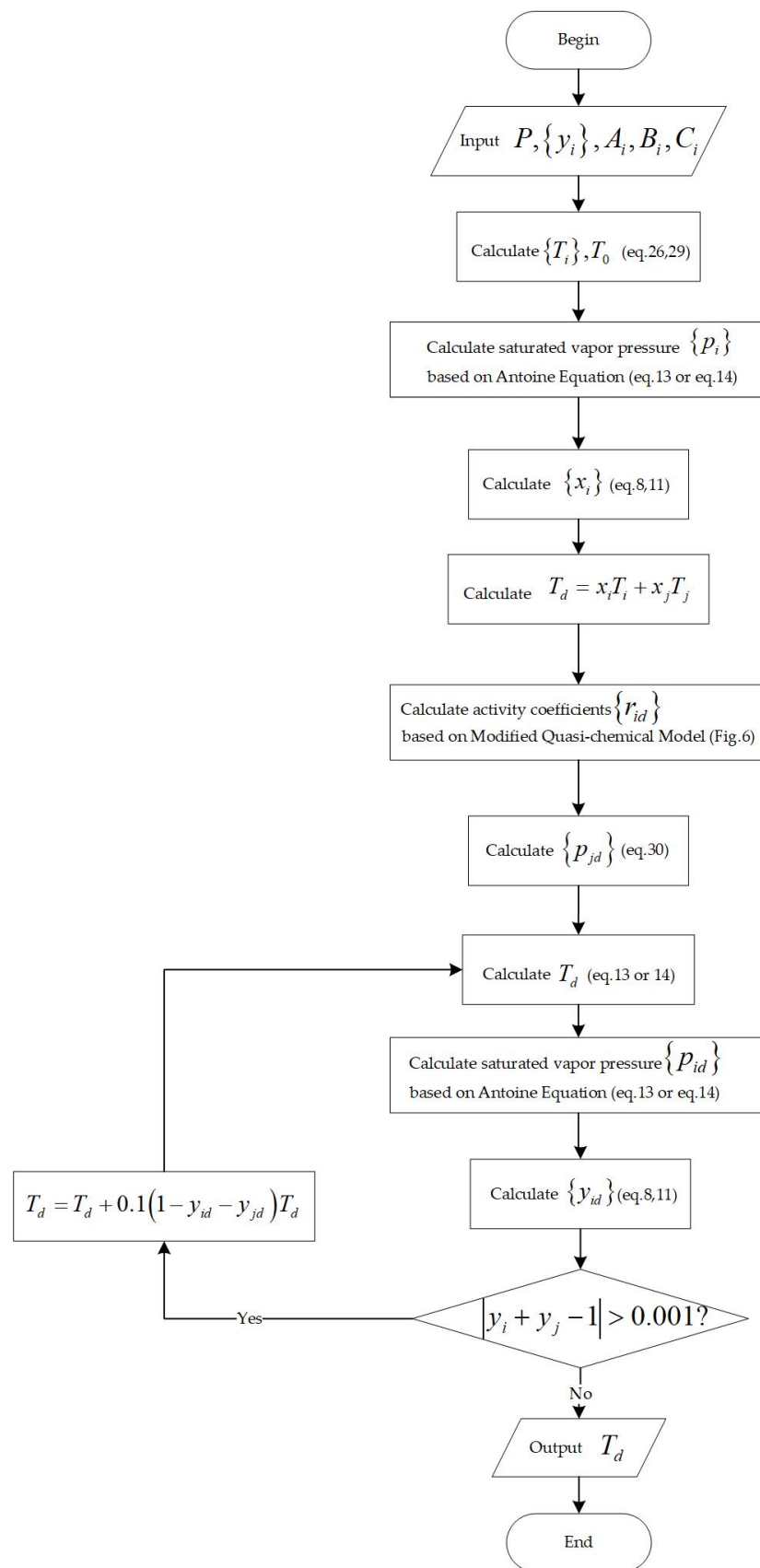


Figure 5. Flowchart for the calculation of dew point temperature.

The activity coefficient can be obtained [35] according to the following relationship between itself and partial molar excess free energy, as shown in Figure 6.

$$\overline{G}_i^E = RT \ln r_i \quad (44)$$

$$\ln r_1 = b_1 z \ln\{(\xi - 1 + 2Y_1)/[Y_1(1 + \xi)]\}/2 - 2b_1 Y_1 Y_2^2 [\partial(\omega - T\eta)/\partial Y_2]/[RT(1 + \xi)] \quad (45)$$

$$\ln r_2 = b_2 z \ln\{(\xi - 1 + 2Y_2)/[Y_2(1 + \xi)]\}/2 + 2b_2 Y_2 Y_1^2 [\partial(\omega - T\eta)/\partial Y_2]/[RT(1 + \xi)] \quad (46)$$

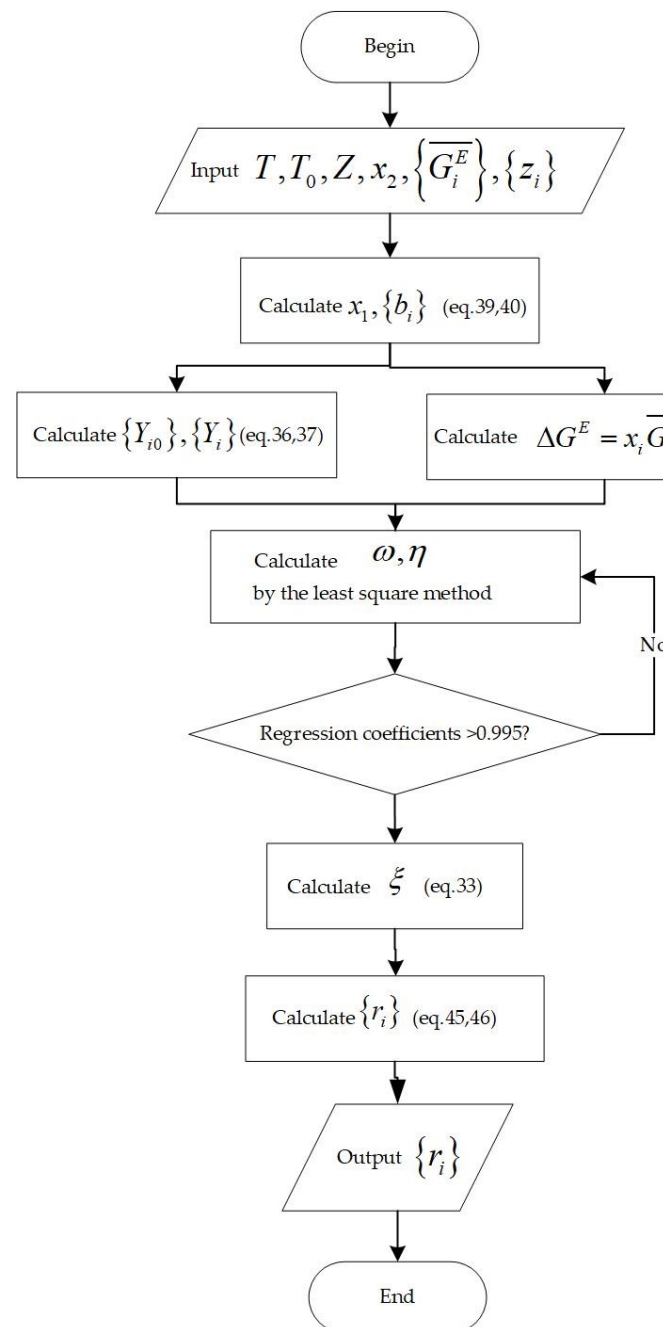


Figure 6. Flowchart for the calculation of activity coefficients.

### 2.3. Materials and Synthesis

After all the components were dried at 393 K in advance in an oven for 24 h, potassium chloride and magnesium chloride (A.R., from Shanghai Aladdin Biochemical Technol-

ogy Co. Ltd., Shanghai, China) and sodium chloride and calcium chloride (A.R., from Guangzhou Chemical Reagent Technology Co. Ltd., Guangzhou, China) were combined in pairs to prepare five binary chloride molten salts with a corresponding mole mass ratio using the static melting method [36]. Further, five groups of two different salts were fully and evenly mixed in five corundum crucibles after being ground and crushed, and were heated using a muffle furnace from the ambient temperature (305 K) to a temperature 423 K higher than the lowest eutectic point at a heating rate of 5 K/min. The salts were fused into a homogeneous mixture, held at that temperature for 10 h, and then cooled at ambient temperature (305 K) before being ground into powder, sealed, and stored in a vacuumed desiccator.

2.4. Measurements and Procedure

At present, researchers mostly use TGA to analyze the thermal stability of molten salt. When the thermal weight loss curve is significantly reduced, the corresponding temperature can be defined as the upper limit of the working temperature of the molten salt.

In this paper, the experimental value of the maximum operating temperature of five chloride salts was obtained by a thermal gravimetric analyzer (PerkinElmer STA 8000). All five chloride molten salts were heated to 1273 K at a rate of 20 K/min with a platinum crucible in a highly purified nitrogen atmosphere at a flow rate of 100 mL/min.

3. Results and Discussion

3.1. Verification of the Modified Quasi-Chemical Model in Binary Chloride Molten Salts System

Through  $\omega$  and  $\eta$ , the thermodynamic quantities of chloride molten salts can be calculated using the modified quasi-chemical model. For the NaCl-KCl binary chloride molten salt system,  $z = 6$ ,  $\epsilon = \frac{1}{2}$ ,  $b_1 = 0.3333$ , and  $b_2 = 0.3333$ , and the multinomial expressions of  $\omega$  and  $\eta$  at 1083 K were obtained as follows, supported by literature data [37]:

$$\omega = 0.036179 - 0.06599Y_2 + 0.027465Y_2^2 + 0.015558Y_2^3 - 0.01569Y_2^4 + 0.003203Y_2^5 - 0.00443Y_2^6 \text{ (J/mol)} \tag{47}$$

$$\eta = -39.1822 + 71.46415Y_2 - 29.7441Y_2^2 - 16.849Y_2^3 + 16.99621Y_2^4 - 3.46882Y_2^5 + 4.799909Y_2^6 \text{ (J/mol)} \tag{48}$$

The activity coefficients of the NaCl-KCl system at 1083 K were calculated by substituting Equations (47) and (48) into (45) and (46) as shown in Figure 7. The activities of the NaCl-KCl system were calculated using the relationship between activity and the activity coefficient illustrated in Equation (49), as shown in Table 1. Figure 8 depicts the comparison results of calculated values and literature data.

$$a_i = x_i \gamma_i \tag{49}$$

**Table 1.** Calculated activity values and literature data of the NaCl-KCl binary chloride system at 1083 K.

NaCl-KCl at 1083 K				
$x_{KCl}$	$a_{NaCl-lit}$	$a_{NaCl-cal}$	$a_{KCl-lit}$	$a_{KCl-cal}$
0.1	0.898	0.896	0.086	0.088
0.2	0.794	0.797	0.177	0.175
0.3	0.695	0.690	0.267	0.271
0.4	0.582	0.584	0.371	0.370
0.5	0.477	0.479	0.477	0.471
0.6	0.371	0.373	0.580	0.578
0.7	0.270	0.271	0.687	0.686
0.8	0.172	0.175	0.796	0.792
0.9	0.084	0.082	0.899	0.902

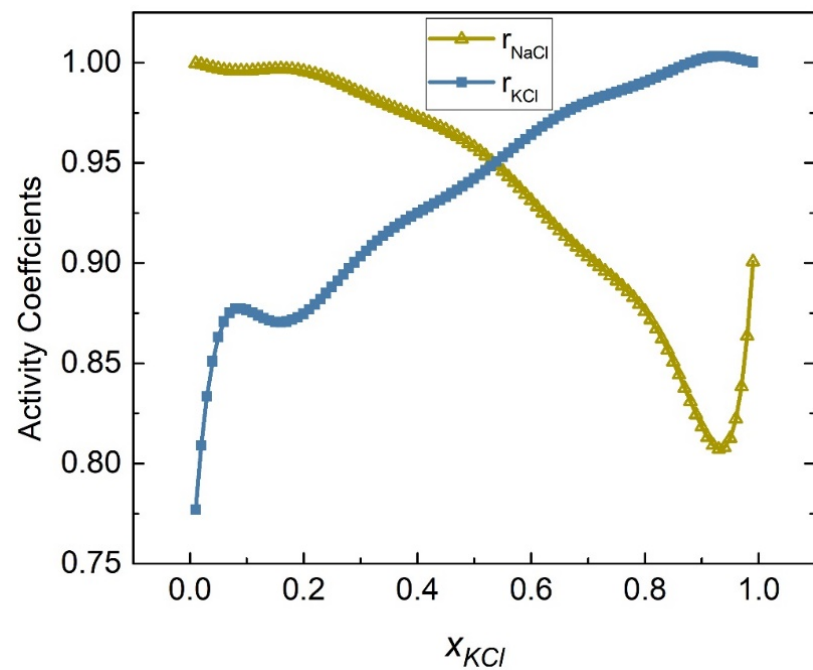


Figure 7. Calculated activity coefficients of each element of the NaCl-KCl system (1083 K).

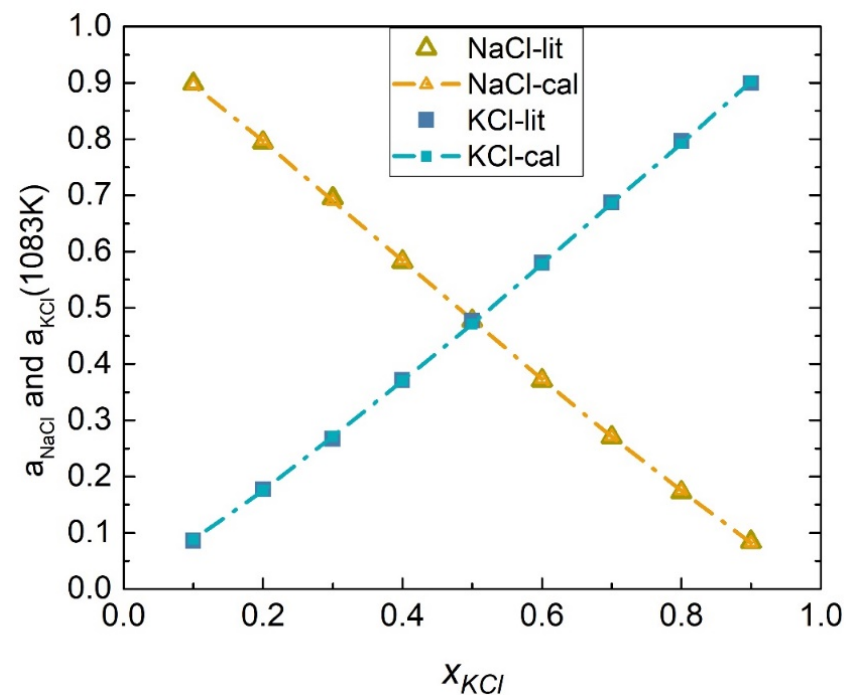


Figure 8. Comparison of the calculated activities and literature data of each element of the NaCl-KCl system (1083 K).

The average relative deviation (ARD)  $S_i^*$  and standard deviation (SD)  $S_i$  were introduced to measure the approximation between the calculated values and the literature data,

$$S_i^* = \pm(100/n) \sum_{i=1}^n |(a_{i,cal} - a_{i,lit}) / a_{i,lit}| \quad (50)$$

$$S_i = \pm \sqrt{\left[ \sum_{i=1}^n (a_{i,cal} - a_{i,lit})^2 \right] / n} \tag{51}$$

where  $n$  is the number of literature data,  $a_{i,cal}$  and  $a_{i,lit}$  represent the calculated value and literature data of activities of component  $i$ , respectively. The calculation results, at 1083 K, showed that the SD and ARD of component NaCl were 0.00267 and 0.052%, while the SD and ARD of KCl were 0.00318 and 0.056%.

For the NaCl-CaCl<sub>2</sub> binary chloride molten salt system,  $z = 6$ ,  $\epsilon = \frac{1}{2}$ ,  $b_1 = 0.3333$ , and  $b_2 = 0.3333$ , and the multinomial expressions of  $\omega$  and  $\eta$  at 998 K, supported by literature data [38], were obtained as follows:

$$\omega = 27.64323 - 99.7584Y_2 + 149.3453Y_2^2 - 120.03Y_2^3 + 55.81855Y_2^4 - 15.011Y_2^5 + 2.180184Y_2^6 - 0.1692Y_2^7 \text{ (J/mol)} \tag{52}$$

$$\eta = -27587.9 + 99558.88Y_2 - 149047Y_2^2 + 119789.9Y_2^3 - 55706.9Y_2^4 + 14981.02Y_2^5 - 2175.82Y_2^6 + 168.865Y_2^7 \text{ (J/mol)} \tag{53}$$

The activity coefficients of the NaCl-CaCl<sub>2</sub> system at 998 K were calculated by substituting Equations (52) and (53) into (45) and (46), as shown in Figure 9. Table 2 shows the calculated activities of the NaCl-CaCl<sub>2</sub> system, and Figure 10 shows the comparison results of calculated values and literature data. The SD and ARD of component NaCl were 0.01282 and 5.888%, respectively, whereas the SD and ARD of CaCl<sub>2</sub> were 0.02815 and 0.71%.

Similarly, for the KCl-CaCl<sub>2</sub> binary chloride molten salt system,  $z = 6$ ,  $\epsilon = \frac{1}{2}$ ,  $b_1 = 0.3333$ , and  $b_2 = 0.3333$ , and the multinomial expressions of  $\omega$  and  $\eta$  at 1058 K, supported by literature data [39], were obtained as follows:

$$\omega = -1.09632 + 3.493849Y_2 - 4.33233Y_2^2 + 2.639964Y_2^3 - 0.87714Y_2^4 + 0.191135Y_2^5 - 0.0802Y_2^6 \text{ (J/mol)} \tag{54}$$

$$\eta = 1159.908 - 3696.49Y_2 + 4583.605Y_2^2 - 2793.08Y_2^3 + 928.0193Y_2^4 - 202.221Y_2^5 + 84.85492Y_2^6 \text{ (J/mol)} \tag{55}$$

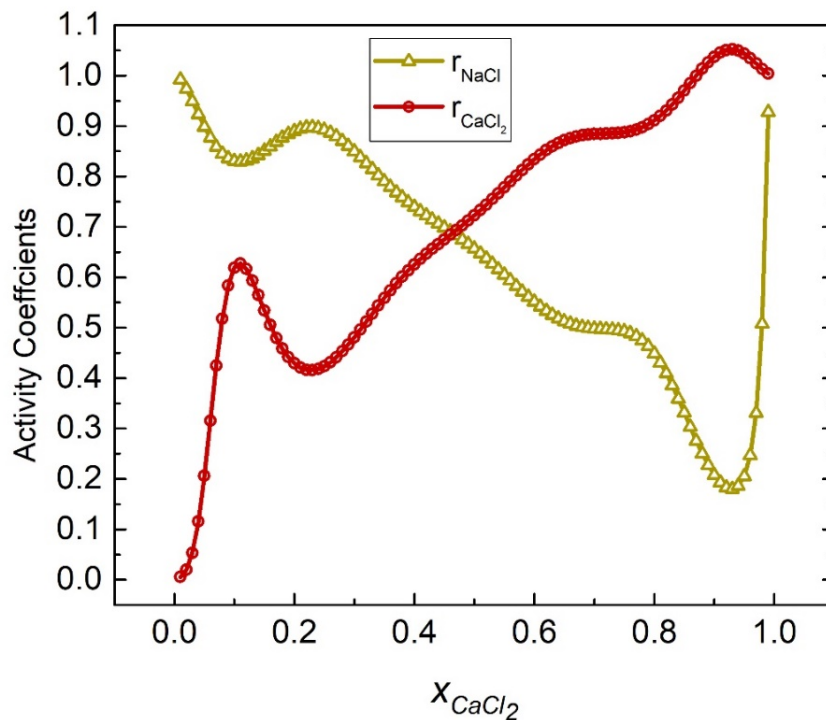
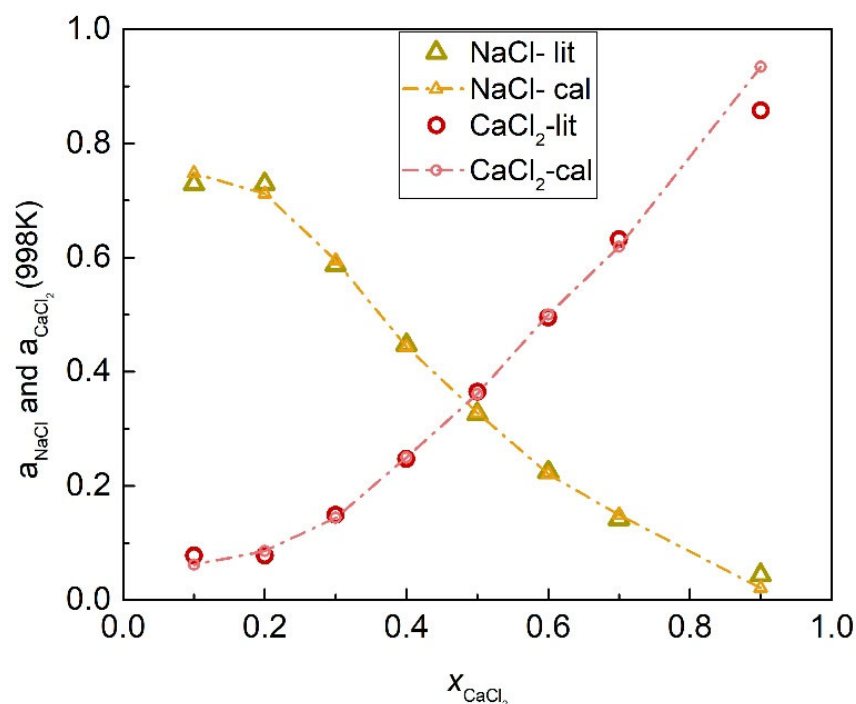


Figure 9. Calculated activity coefficients of each element of the NaCl-CaCl<sub>2</sub> system (998 K).



**Figure 10.** Comparison of the calculated activities and literature data of each element of the NaCl-CaCl<sub>2</sub> system (998 K).

**Table 2.** Calculated activity values and FactSage data of the NaCl-CaCl<sub>2</sub> binary chloride system at 998 K.

NaCl-CaCl <sub>2</sub> at 998 K				
$x_{CaCl_2}$	$a_{NaCl-fac}$	$a_{NaCl-cal}$	$a_{CaCl_2-fac}$	$a_{CaCl_2-cal}$
0.1	0.729	0.748	0.078	0.062
0.2	0.729	0.712	0.078	0.086
0.3	0.587	0.595	0.149	0.144
0.4	0.447	0.444	0.247	0.250
0.5	0.326	0.328	0.365	0.361
0.6	0.224	0.221	0.495	0.500
0.7	0.142	0.149	0.632	0.619
0.9	0.044	0.021	0.858	0.934

The activities coefficients of the KCl-CaCl<sub>2</sub> system at 1058 K were calculated by substituting Equations (54) and (55) into (45) and (46), respectively, as shown in Figure 11. Table 3 shows the calculated activities of the KCl-CaCl<sub>2</sub> system, and Figure 12 shows the comparison results of calculated values and literature data. The SD and ARD of component KCl were 0.00775 and 1.806%, respectively, while the SD and ARD of CaCl<sub>2</sub> were 0.00727 and 5.75%, respectively.

For the NaCl-MgCl<sub>2</sub> binary chloride molten salt system,  $z = 6$ ,  $\varepsilon = \frac{1}{3}$ ,  $b_1 = 0.2294$ , and  $b_2 = 0.4594$ , and the multinomial expressions of  $\omega$  and  $\eta$  at 1098 K, supported by literature data [39], were obtained as follows:

$$\omega = -0.99823 + 2.031157Y_2 - 1.45713Y_2^2 + 0.405384Y_2^3 - 0.09392Y_2^4 \text{ (J/mol)} \quad (56)$$

$$\eta = 1096.053 - 2230.21Y_2 + 1599.928Y_2^2 - 445.112Y_2^3 + 103.1219Y_2^4 \text{ (J/mol)} \quad (57)$$

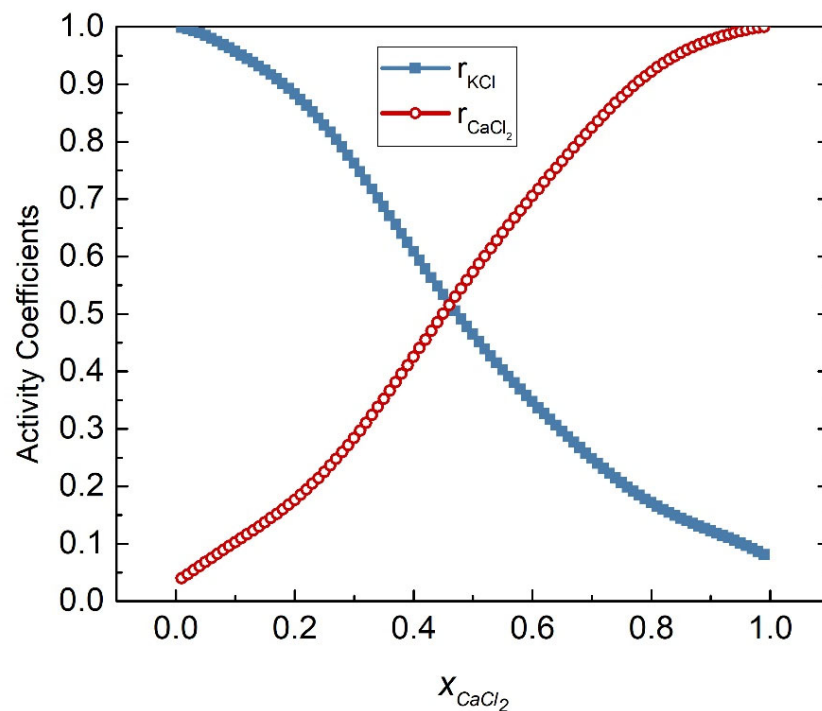


**Figure 11.** Calculated activity coefficients of each element of the KCl-CaCl<sub>2</sub> system (1058 K).

**Table 3.** Calculated activity values and literature data of the KCl-CaCl<sub>2</sub> binary chloride system at 1058 K.

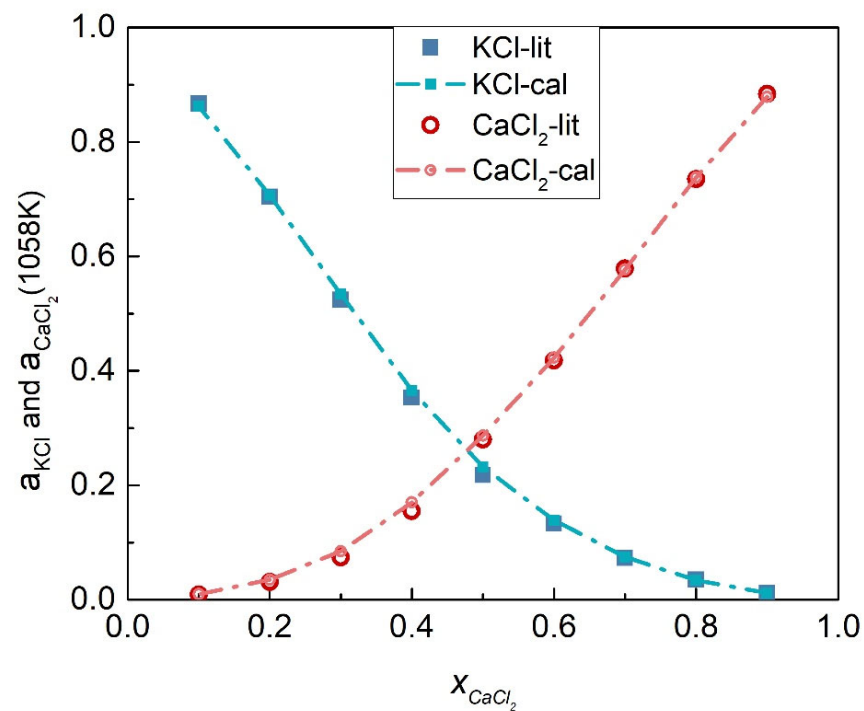
KCl-CaCl <sub>2</sub> at 1058 K				
$x_{CaCl_2}$	$a_{KCl-lit}$	$a_{KCl-cal}$	$a_{CaCl_2-lit}$	$a_{CaCl_2-cal}$
0.1	0.867	0.862	0.009	0.010
0.2	0.704	0.707	0.031	0.035
0.3	0.524	0.534	0.074	0.085
0.4	0.353	0.366	0.155	0.170
0.5	0.218	0.232	0.280	0.287
0.6	0.133	0.139	0.418	0.423
0.7	0.073	0.075	0.579	0.577
0.8	0.035	0.034	0.735	0.738
0.9	0.012	0.012	0.884	0.879

The activities coefficients of the NaCl-MgCl<sub>2</sub> system at 1098 K were calculated by substituting Equations (56) and (57) into (45) and (46), respectively, as shown in Figure 13. Table 4 shows the calculated activities of the NaCl-MgCl<sub>2</sub> system, and Figure 14 shows the comparison results of calculated values and literature data. The SD and ARD of component NaCl were 0.01642 and 2.884%, respectively, while the SD and ARD of component MgCl<sub>2</sub> were 0.01696 and 6.604%, respectively.

For the KCl-MgCl<sub>2</sub> binary chloride molten salt system,  $z = 6$ ,  $\varepsilon = \frac{1}{3}$ ,  $b_1 = 0.2294$ , and  $b_2 = 0.4594$ , and the multinomial expressions of  $\omega$  and  $\eta$  at 998 K were obtained, supported by literature data [39], as follows:

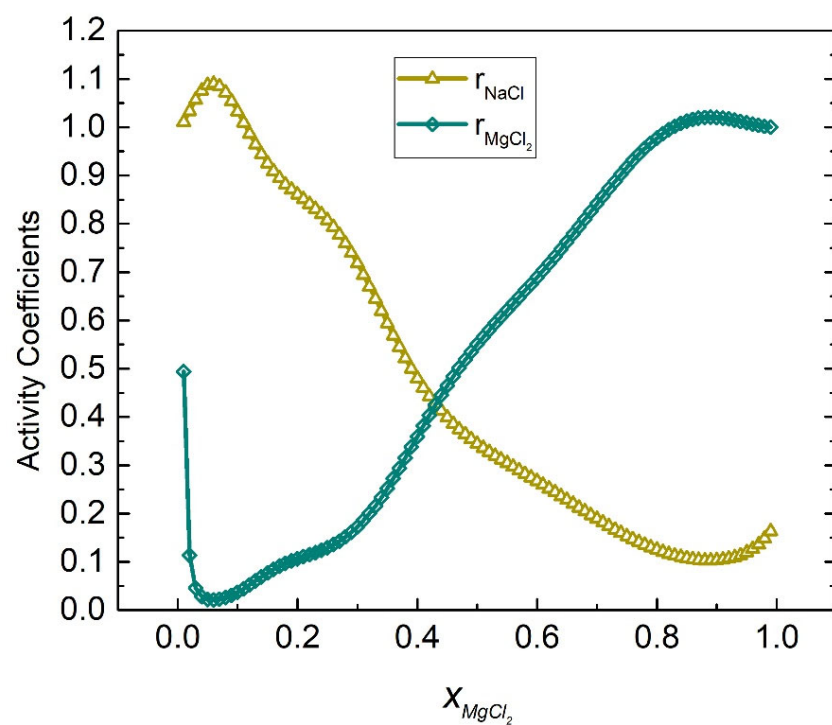
$$\omega = -0.17975 - 0.46824Y_2 + 2.864088Y_2^2 - 4.12313Y_2^3 + 2.346907Y_2^4 - 0.55023Y_2^5 - 0.07127Y_2^6 \text{ (J/mol)} \quad (58)$$

$$\eta = 179.3948 + 467.302Y_2 - 2858.36Y_2^2 + 4114.884Y_2^3 - 2342.21Y_2^4 + 549.1279Y_2^5 + 71.12457Y_2^6 \text{ (J/mol)} \quad (59)$$



**Figure 12.** Comparison of the calculated activities and literature data of each element of the KCl-CaCl<sub>2</sub> system (1058 K).

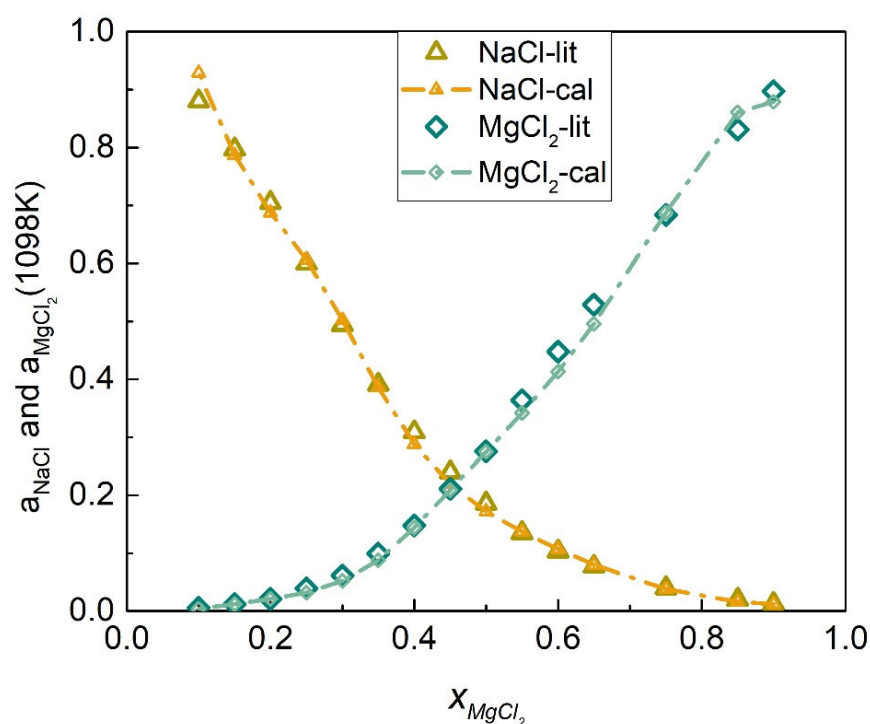
The activity coefficients of the KCl-MgCl<sub>2</sub> system at 998 K were calculated by substituting Equations (58) and (59) into (45) and (46), respectively, as shown in Figure 15. Table 5 shows the calculated activities of the KCl-MgCl<sub>2</sub> system, and Figure 16 shows the comparison results of calculated values and literature data. Furthermore, the SD and ARD of component KCl and MgCl<sub>2</sub> were 0.02200 and 8.014% and 0.008407 and 12.3865%, respectively, which can be found in Table 6.



**Figure 13.** Calculated activity coefficients of each element of the NaCl-MgCl<sub>2</sub> system (1098 K).

**Table 4.** Calculated activity values and literature data of the NaCl-MgCl<sub>2</sub> binary chloride system at 1098 K.

NaCl-MgCl <sub>2</sub> at 1098 K				
$x_{MgCl_2}$	$a_{NaCl-lit}$	$a_{NaCl-cal}$	$a_{MgCl_2-lit}$	$a_{MgCl_2-cal}$
0.10	0.880	0.929	0.006	0.004
0.15	0.797	0.787	0.012	0.012
0.20	0.705	0.688	0.021	0.021
0.25	0.600	0.606	0.039	0.032
0.30	0.494	0.502	0.061	0.052
0.35	0.391	0.386	0.099	0.088
0.40	0.309	0.288	0.148	0.144
0.45	0.240	0.219	0.211	0.209
0.50	0.186	0.172	0.276	0.275
0.55	0.135	0.137	0.364	0.342
0.60	0.103	0.107	0.448	0.413
0.65	0.077	0.080	0.529	0.496
0.75	0.040	0.038	0.684	0.688
0.85	0.020	0.016	0.831	0.861
0.90	0.013	0.012	0.897	0.879

**Figure 14.** Comparison of the calculated activities and literature data of each element of the NaCl-MgCl<sub>2</sub> system (1098 K).

Combined with the above data, it can be shown that the modified quasi-chemical model can fit the bond energy parameters  $\omega$  and  $\eta$  of the components of the binary chloride molten salts systems and calculate their activity coefficient. The modified quasi-chemical model had a good calculation effect on the binary chloride molten salts system, which is in good agreement with the data in the literature according to the error analysis of activity. As a result, the modified quasi-chemical model's calculated data were deemed reliable. According to the bond energy parameters  $\omega$  and  $\eta$  calculated above, the activity coefficients of chloride salts can be obtained at any temperature.

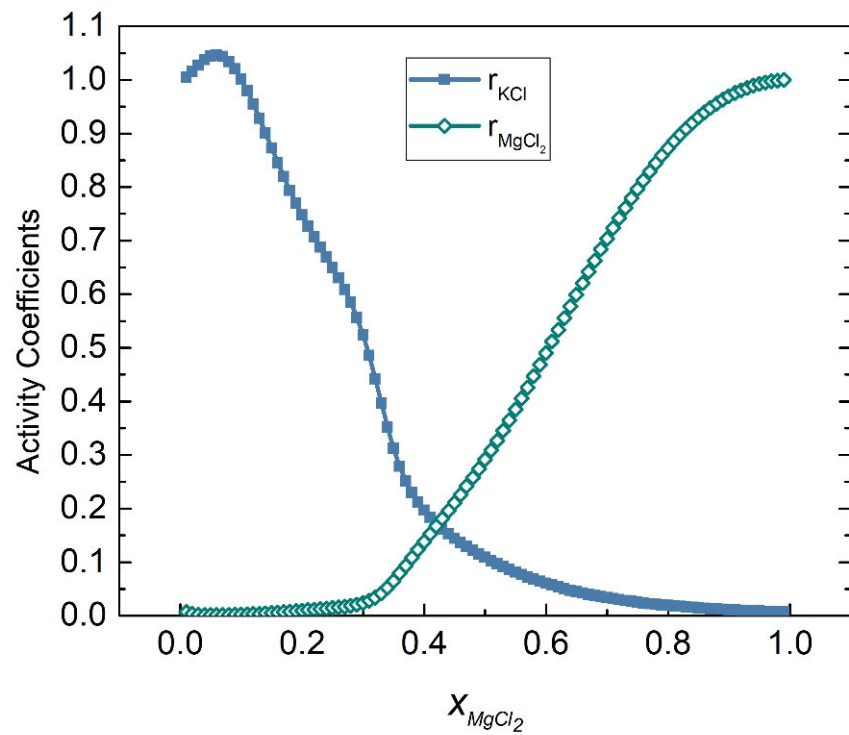


Figure 15. Calculated activity coefficients of each element of the KCl-MgCl<sub>2</sub> system (998 K).

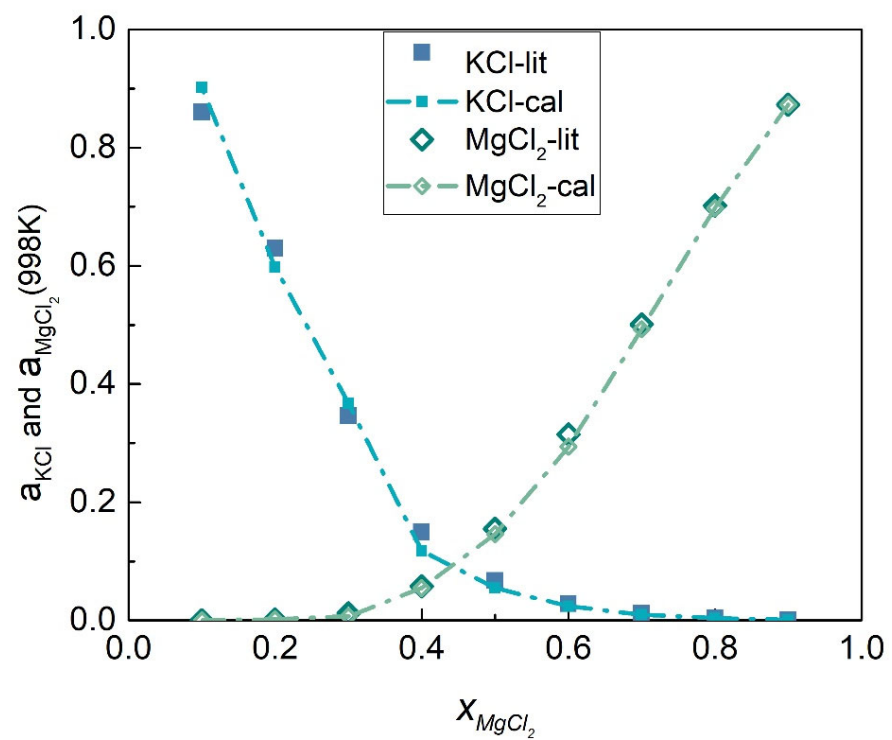


Figure 16. Comparison of calculated activities and literature data of each element of the KCl-MgCl<sub>2</sub> system (998 K).

**Table 5.** Calculated activity values and literature data of the KCl-MgCl<sub>2</sub> binary chloride system at 998 K.

KCl-MgCl <sub>2</sub> at 998 K				
$x_{MgCl_2}$	$a_{KCl-lit}$	$a_{KCl-cal}$	$a_{MgCl_2-lit}$	$a_{MgCl_2-cal}$
0.1	0.860	0.902	0.0004	0.0002
0.2	0.630	0.598	0.002	0.002
0.3	0.346	0.367	0.012	0.007
0.4	0.149	0.118	0.058	0.055
0.5	0.067	0.055	0.155	0.146
0.6	0.028	0.024	0.315	0.294
0.7	0.012	0.010	0.501	0.493
0.8	0.004	0.004	0.702	0.698
0.9	0.0012	0.0011	0.873	0.873

**Table 6.** Average relative deviation and standard deviation of the binary chloride systems.

$i-j$	T/K	$\pm S_{i-cal}$	$\pm S_{j-cal}$	$S_{i-cal}^*$ (%)	$S_{j-cal}^*$ (%)
NaCl-KCl	1083	0.00267	0.00318	0.052	0.056
NaCl-CaCl <sub>2</sub>	998	0.01282	0.02815	5.888	0.710
KCl-CaCl <sub>2</sub>	1058	0.00775	0.00727	1.806	5.750
NaCl-MgCl <sub>2</sub>	1098	0.01642	0.01696	2.884	6.604
KCl-MgCl <sub>2</sub>	998	0.02200	0.00841	8.014	12.387

### 3.2. Calculation of the P-T Phase Diagram

Binary chloride molten salts systems with small and big boiling point difference between the components can be regarded as narrow boiling range systems and wide boiling range systems, respectively. The boiling points and specific heat capacity of common chlorides NaCl, KCl, CaCl<sub>2</sub>, and MgCl<sub>2</sub> are shown in Table 7, obtained from the FactSage software and databases. The NaCl-KCl, NaCl-MgCl<sub>2</sub>, and KCl-MgCl<sub>2</sub> binary chloride molten salt systems are narrow boiling range systems due to the relatively small boiling point difference, whereas the NaCl-CaCl<sub>2</sub> and KCl-CaCl<sub>2</sub> binary chloride molten salt systems are wide boiling range systems due to the relatively large temperature range. The Antoine constants of NaCl, KCl, CaCl<sub>2</sub>, and MgCl<sub>2</sub> are demonstrated in Table 8 [40,41].

**Table 7.** Physical parameters for the pure salts obtained from FactSage.

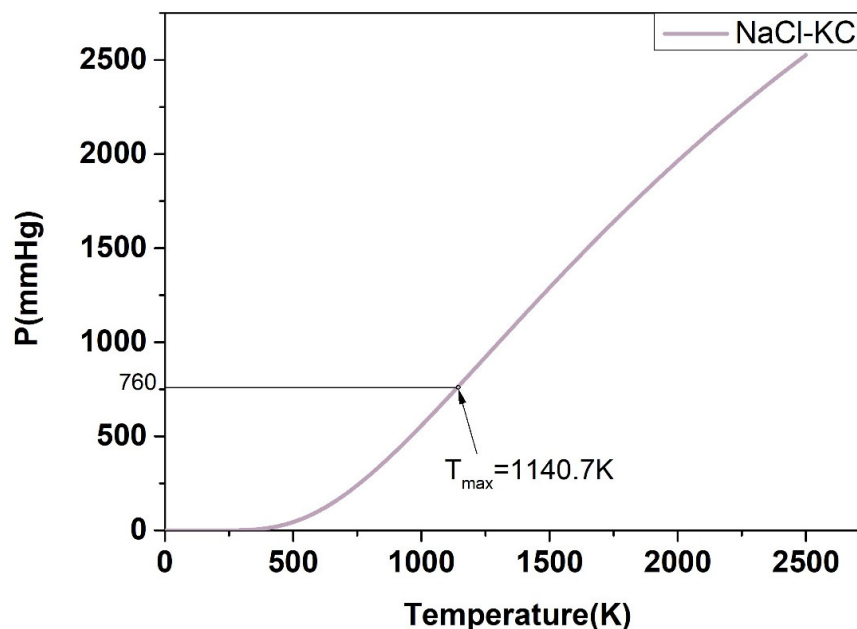
Component	$T_{b.p.}$ K	$C_{pl}$ J/(mol·K)	$C_{pv}$ J/(mol·K)
NaCl	1734	$77.763824 - 7.5312 \times 10^{-3}T$ (298–1500 K) 66.944 (1500–2000 K)	$37.333832 + 7.36384 \times 10^{-4}T - 158573.6T^{-2}$
KCl	1693	73.59656 193.40893 – 0.36201388T	$37.145552 + 9.49768 \times 10^{-4}T - 84098.4T^{-2}$
MgCl <sub>2</sub>	1685	$-3788503.9T^{-2} + 3.19987074T^2$ (298–660 K) 92.048 (660–2500 K)	$62.3647 - 695753.73T^{-2} + 67611239T^{-3}$
CaCl <sub>2</sub>	1873	$81.479332 - 0.00254166793T$ $-2789.1275T^{-1}$ (298–700 K) 102.533 (700–3000 K)	$62.382104 - 100.35854T^{-1} - 244513.85T^{-2}$

**Table 8.** Antoine constants for the pure salts.

Component	Antoine Constant A	Antoine Constant B	Antoine Constant C
NaCl	8.4459	9565	/
KCl	8.28	9032	/
CaCl <sub>2</sub>	8.4073	12622	/
MgCl <sub>2</sub>	23.15	11735	4.076

Combining the relevant thermodynamic data, the P-T phase diagrams of the molten salts NaCl-KCl, NaCl-CaCl<sub>2</sub>, KCl-CaCl<sub>2</sub>, NaCl-MgCl<sub>2</sub>, and KCl-MgCl<sub>2</sub> were calculated using the adiabatic flash calculation theory and modified quasi-chemical model detailed in the previous section according to the flowchart of the wide and narrow boiling range mixtures.

For the P-T phase diagram, the system is in flash equilibrium only when the system pressure is equal to one atmosphere, and the temperature corresponding to the standard atmospheric pressure (760 mmHg) is the evaporation point of the substance. Based on this, as demonstrated in Figures 17–21, the calculated evaporation temperature of NaCl-KCl, NaCl-CaCl<sub>2</sub>, KCl-CaCl<sub>2</sub>, NaCl-MgCl<sub>2</sub>, and KCl-MgCl<sub>2</sub>, corresponding to the standard atmospheric pressure, were 1140.7 K, 1150.6 K, 1176.4 K, 1085.5 K, and 1067.9 K, at which the molten salts are in flash equilibrium. Before these temperature points, the eutectic chloride molten salts above are in liquid phase, while after these temperature points, the chloride molten salts are expected to gradually evaporate as they transition from liquid to vapor. When the evaporation process began, the weight of the chloride molten salts began to fall sharply. When the weight of the chloride molten salts dropped to a certain extent in the actual service conditions, the corresponding temperature at that time was identified as the maximum working temperature of the molten salts, which also reflects the thermal stability of the molten salts.

**Figure 17.** Calculated P-T phase diagram of the NaCl-KCl binary system.

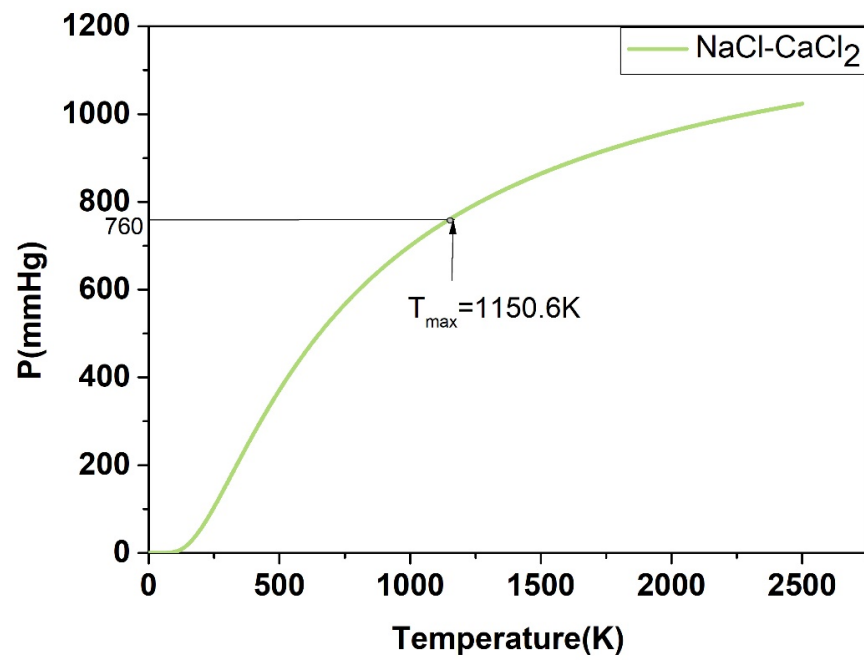


Figure 18. Calculated P-T phase diagram of the NaCl-CaCl<sub>2</sub> binary system.

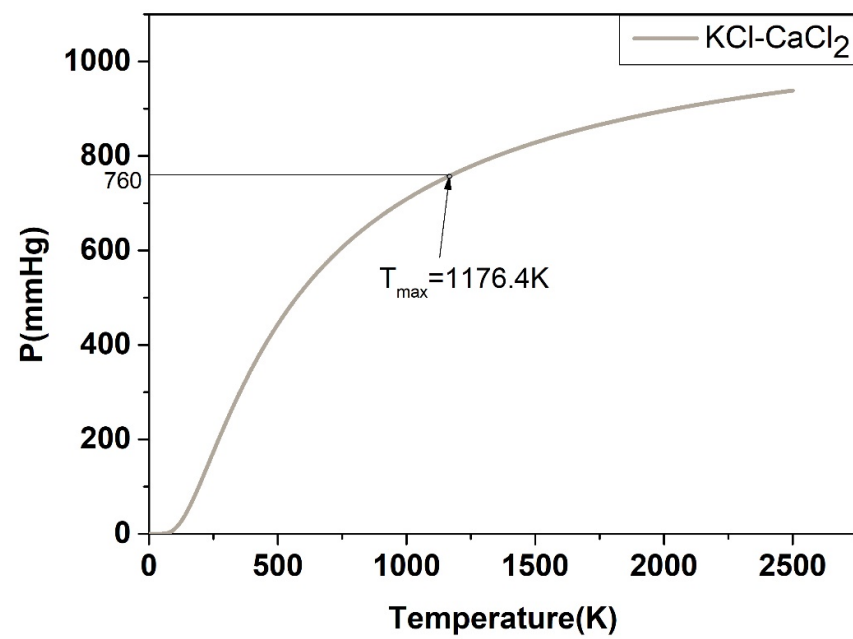


Figure 19. Calculated P-T phase diagram of the KCl-CaCl<sub>2</sub> binary system.

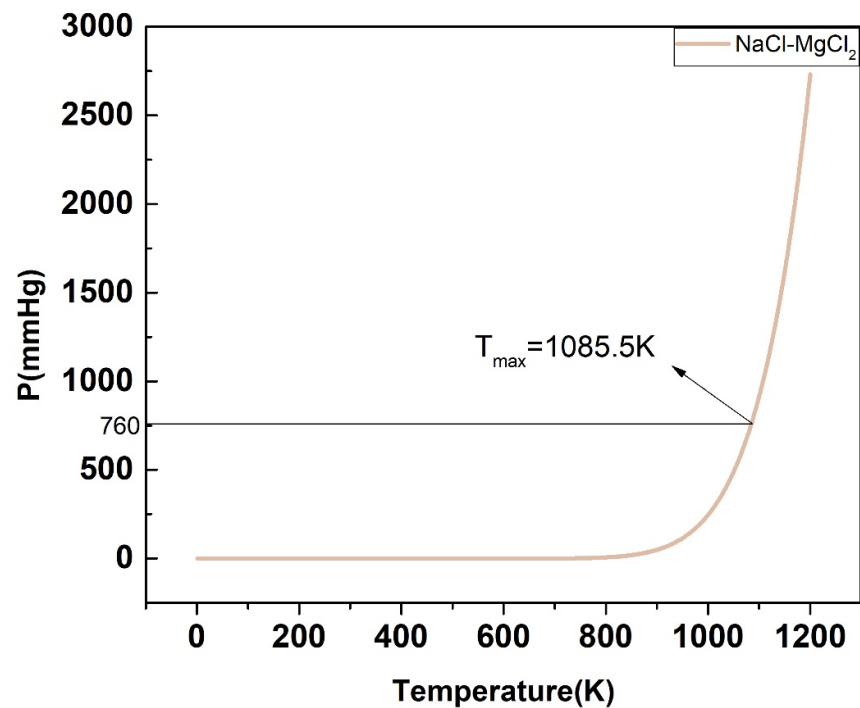


Figure 20. Calculated P-T phase diagram of the NaCl-MgCl<sub>2</sub> binary system.

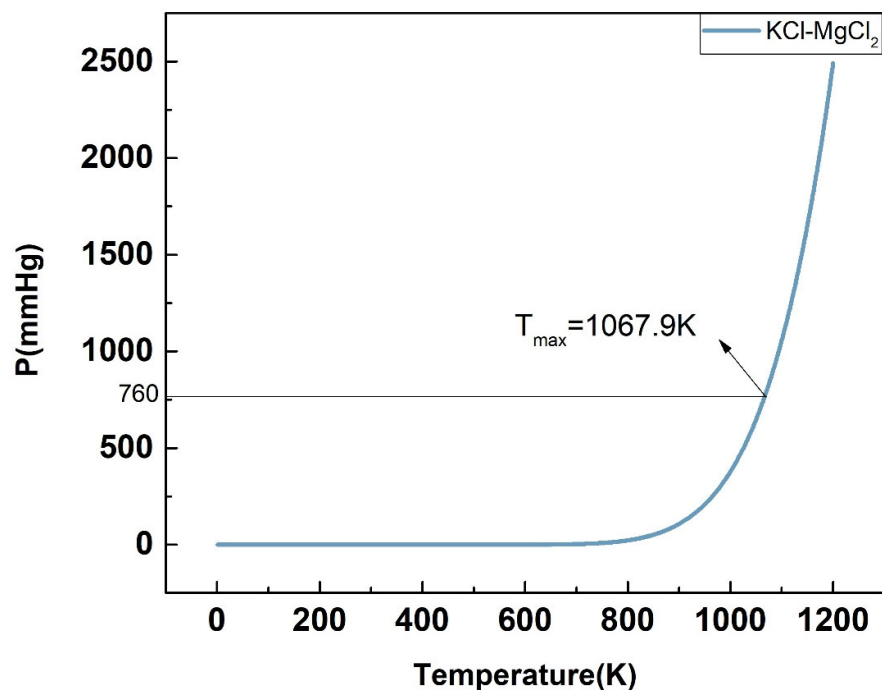


Figure 21. Calculated P-T phase diagram of the KCl-MgCl<sub>2</sub> binary system.

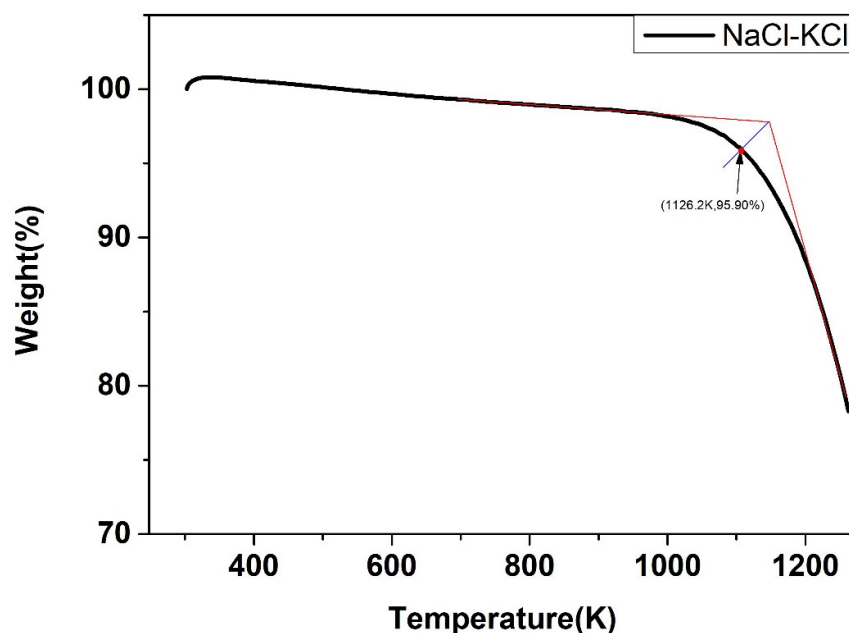
### 3.3. Thermal Gravimetric Analysis of the Binary Chloride Salts

As shown in Table 9, the molar mass ratio corresponding to the lowest eutectic temperature of NaCl-KCl, NaCl-CaCl<sub>2</sub>, KCl-CaCl<sub>2</sub>, NaCl-MgCl<sub>2</sub>, and KCl-MgCl<sub>2</sub> chloride molten salts was obtained, referring to the FactSage software. The five salts were prepared according to the ratio and were then taken into the TGA.

**Table 9.** Lowest eutectic temperature and molar mass ratio of the binary chloride salts from FactSage.

Species	Lowest Eutectic Temperature K	Molar Mass Ratio
NaCl-KCl	841.14	0.47:0.53
NaCl-CaCl <sub>2</sub>	749.7	0.51:0.49
KCl-CaCl <sub>2</sub>	874.4	0.75:0.25
NaCl-MgCl <sub>2</sub>	732.16	0.57:0.43
KCl-MgCl <sub>2</sub>	695.69	0.7:0.3

The weight change of the five salts after certain thermal treatment, obtained by the thermal gravimetric analyzer, were shown below. As shown in Figures 22–26, the weight of the five types of chloride molten salts was similarly lost sharply above a certain temperature point. As a result, these temperatures are thought to be the highest working temperatures of chloride molten salts. Results show that the experimental values of the highest working temperature of NaCl-KCl, NaCl-CaCl<sub>2</sub>, KCl-CaCl<sub>2</sub>, NaCl-MgCl<sub>2</sub>, and KCl-MgCl<sub>2</sub> were 1126.2 K, 1117.9 K, 1124.1 K, 1023.9 K, and 1017.9 K, respectively. The mass loss of the five salts at their respective maximum operating temperatures was 4.1%, 12.55%, 11.33%, 19.69%, and 8.5%. The error between the calculated values and experimental values after comparison was 1.29%, 2.93%, 4.65%, 6.02%, and 4.91%, respectively, as shown in Table 10.

**Figure 22.** Weight change (wt.%) of the NaCl-KCl binary chloride salt.**Table 10.** Calculated and experimental value of the upper-temperature limit of the binary chloride salts.

Species	Calculated Value of Upper-Temperature Limit K	Experimental Value of Upper-Temperature Limit K	Relative Error %
NaCl-KCl	1140.7	1126.2	1.29
NaCl-CaCl <sub>2</sub>	1150.6	1117.9	2.93
KCl-CaCl <sub>2</sub>	1176.4	1124.1	4.65
NaCl-MgCl <sub>2</sub>	1085.5	1023.9	6.02
KCl-MgCl <sub>2</sub>	1067.9	1017.9	4.91

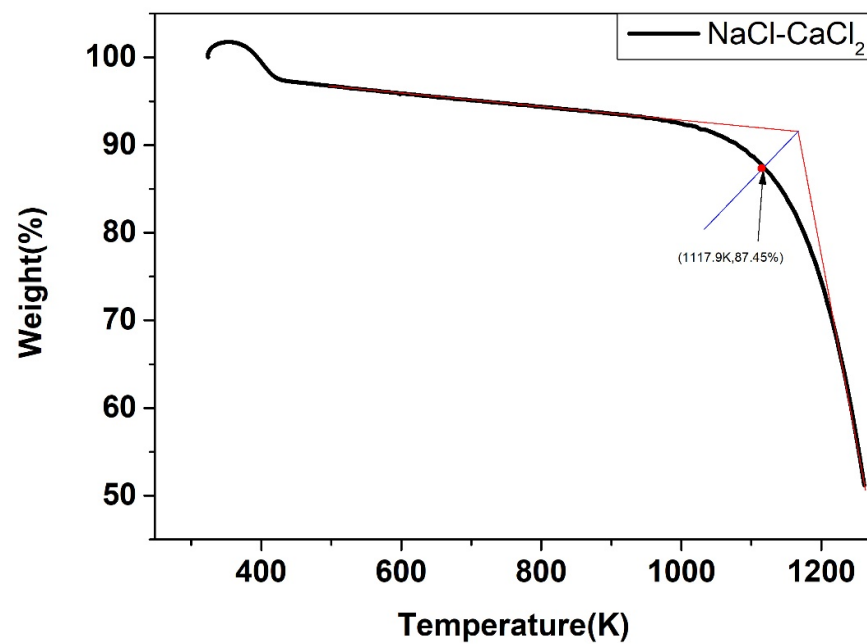


Figure 23. Weight change (wt.%) of the NaCl-CaCl<sub>2</sub> binary chloride salt.

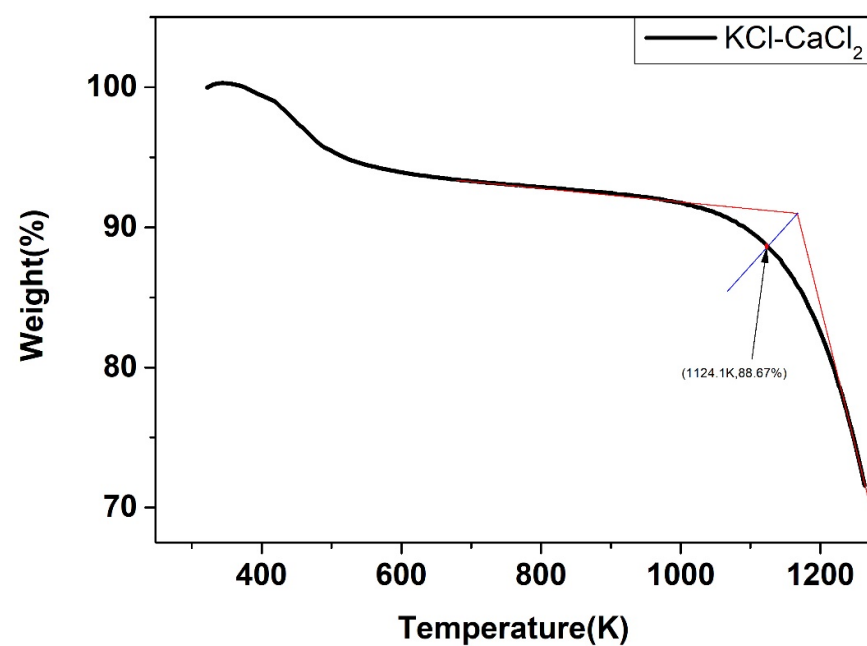


Figure 24. Weight change (wt.%) of the KCl-CaCl<sub>2</sub> binary chloride salt.

Because the maximum error between the calculated value and the experimental value of the maximum operating temperature was 6.02%, while the minimum was 1.29%, which is relatively small, we could consider that the calculation of the maximum operating temperature in this work is relatively accurate.

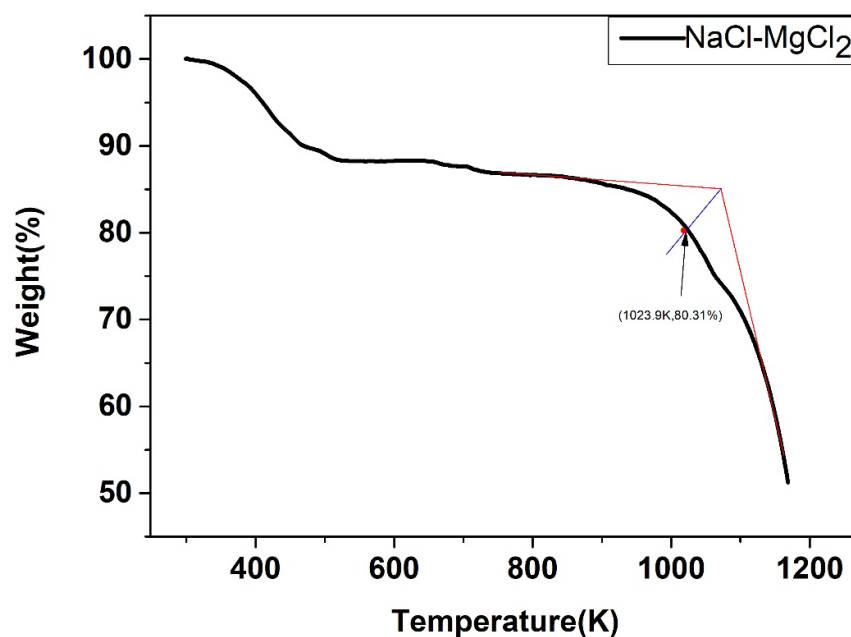


Figure 25. Weight change (wt.%) of the NaCl-MgCl<sub>2</sub> binary chloride salt.

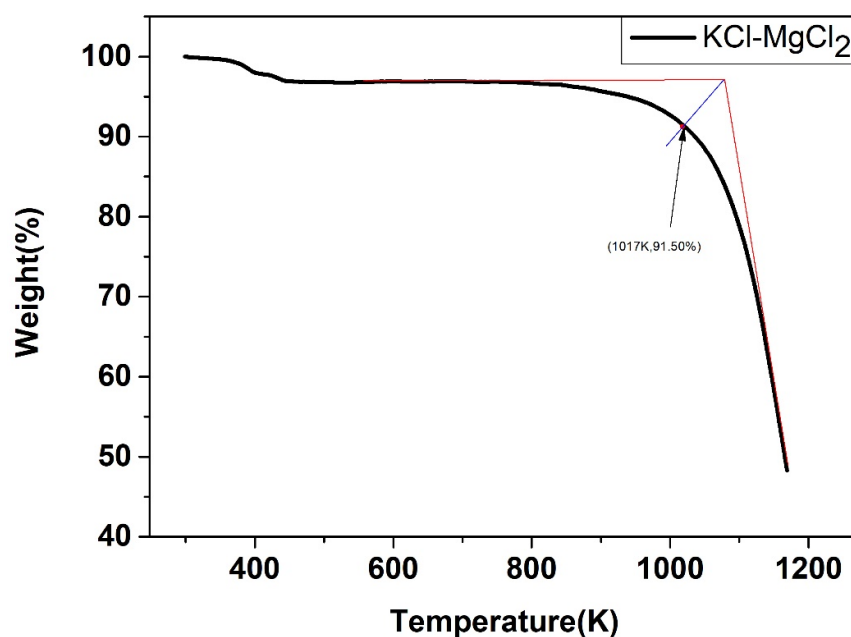


Figure 26. Weight change (wt.%) of the KCl-MgCl<sub>2</sub> binary chloride salt.

#### 4. Conclusions

In this paper, the thermodynamic values of different binary chloride molten salt systems were calculated using the modified quasi-chemical model. The maximum SD between the calculated activity and the literature activity was 0.02815, while the minimum was 0.00267, demonstrating that the modified quasi-chemical model has a high degree of accuracy. Combining the modified quasi-chemical model, the Antoine equation, and the adiabatic flash evaporation calculation principle, the P-T phase diagram of binary chloride molten salts were obtained and the evaporation temperatures of NaCl-KCl, NaCl-CaCl<sub>2</sub>, KCl-CaCl<sub>2</sub>, NaCl-MgCl<sub>2</sub>, and KCl-MgCl<sub>2</sub> were 1140.7 K, 1150.6 K, 1176.4 K, 1085.5 K, and 1067.9 K. The maximum operating temperatures measured experimentally were 1126.2 K, 1117.9 K, 1124.1 K, 1023.9 K, and 1017.9 K. Accordingly, the relative error between the theoretically estimated and experimental values was 1.29%, 2.93%, 4.65%, 6.02%, and 4.91%

for each system. As a result, the method is deemed extremely useful in determining the upper limit of the working temperature of binary chloride salts.

Based on these results, the upper-temperature limits of NaCl-KCl, NaCl-CaCl<sub>2</sub>, KCl-CaCl<sub>2</sub>, NaCl-MgCl<sub>2</sub>, and KCl-MgCl<sub>2</sub> are determined to be 1141 K, 1151 K, 1176 K, 1086 K, and 1068 K. Consequently, the upper limit of the working temperature of the wide boiling range system for the alkali metal-alkaline earth metal binary chloride molten salt systems is higher than that of the narrow boiling range system. Because NaCl and KCl belong to the same main group and have similar properties, the upper limit of the operating temperature of NaCl-KCl is also higher, although it has a narrow boiling range.

The lower limit of the working temperature should be about 50 K higher than the lowest eutectic point, which was demonstrated in Table 9. Combined with the lowest eutectic temperature and the upper-temperature limits of binary chloride molten salts, the stable operating temperature ranges of NaCl-KCl, NaCl-CaCl<sub>2</sub>, KCl-CaCl<sub>2</sub>, NaCl-MgCl<sub>2</sub>, and KCl-MgCl<sub>2</sub> are 891~1141 K, 750~1151 K, 874~1176 K, 732~1086 K, and 696~1086 K, and NaCl-CaCl<sub>2</sub>, NaCl-MgCl<sub>2</sub>, and KCl-MgCl<sub>2</sub> binary molten chlorides have a wider working temperature range. Therefore, in practical applications, the types of chloride molten salts used in different temperature sections can be adjusted according to the optimal working temperature range of different chloride molten salts. Furthermore, this article provides an idea for accurately predicting the maximum operating temperature using the computation method, which could hopefully promote the commercial application of chloride molten salts.

**Author Contributions:** Conceptualization, J.D., J.L. and X.W.; formal analysis, J.Z.; funding acquisition, J.D., J.L. and W.W.; investigation, J.Z.; methodology, J.Z.; resources, J.D. and W.W.; supervision, J.D.; validation, J.Z.; writing—original draft, J.Z.; writing—review and editing, X.W. and W.W. All authors have read and agreed to the published version of the manuscript.

**Funding:** This research was funded by the funding of the National Natural Science Foundation of China (52036011), Natural Science Foundation of Guangdong Province (2017B030308004), and National Natural Science Foundation of China (U1707603).

**Institutional Review Board Statement:** Not applicable.

**Informed Consent Statement:** Not applicable.

**Data Availability Statement:** The data are not publicly available because it is part of the current research work.

**Conflicts of Interest:** The authors declare no conflict of interest.

## Nomenclature

$A_i$	Antoine constants of component $i$
$B_i$	Antoine constants of component $i$
$C_i$	Antoine constants of component $i$
$C_{pl_i}$	Liquid specific heat capacity of component $i$
$C_{pv_i}$	Vapor specific heat capacity of component $i$
$F$	Total amount of the system
$G^E$	Molar excess free energy
$\overline{G}_i^E$	Partial molar excess free energy of component $i$
$H_F$	Molar enthalpies of the mixture
$H_l$	Molar enthalpies of the liquid
$H_v$	Molar enthalpies of the vapor
$HT$	Enthalpy change
$H_0$	Molar enthalpy of the system before operation
$K_i$	Vapor-liquid equilibrium ratio of component $i$
$P$	System pressure (mmHg)
$Q$	Endothermic heat of the process

$R$	Thermodynamic constant
$S_i$	Standard deviation (SD)
$S_i^*$	Average relative deviation (ARD)
$T$	Temperature (K)
$T_b$	Bubble point temperature
$T_d$	Dew point temperature
$T_i^s$	Saturated temperature of the component $i$
$T_0$	Initial value of $T$
$V_i^l$	Molar volume of pure component $i$
$Y_i$	Equivalent fraction
$a_i$	Activity of component $i$
$a_{i,cal}$	Calculated value of activities of component $i$
$a_{i,lit}$	Literature data of activities of component $i$
$b_1$	Constant of equivalent fraction
$b_2$	Constant of equivalent fraction
$dHT$	Derivative of enthalpy change
$f_i^L$	Fugacity of component $i$ in the liquid phase
$f_i^V$	Fugacity of component $i$ in the vapor phase
$n$	Number of literature data
$p_i$	Vapor pressure of component $i$
$p_i^s$	Saturated vapor pressure of component $i$
$p_{id}$	Saturated vapor pressure of component $i$ in dew point temperature calculation
$p_{jb}$	Saturated vapor pressure of component $j$ in bubble point temperature calculation
$p_{jd}$	Saturated vapor pressure of component $j$ in dew point temperature calculation
$r_i$	Activity coefficient of component $i$ in the liquid phase
$r_{id}$	Activity coefficient of component $i$ in dew point temperature calculation
$v$	Vaporization rate
$x_i$	Mole fraction of component $i$ in the liquid phase
$y_i$	Mole fraction of component $i$ in the vapor phase
$y_{id}$	Mole fraction of component $i$ in the vapor phase in dew point temperature calculation
$z$	Coordination number
$z_i$	Total composition before operation of component $i$
$\Phi_i^*$	Fugacity coefficient of component $i$ in the liquid phase
$\Phi_i^s$	Saturated liquid fugacity coefficient of component $i$
$\Phi_i^v$	Fugacity coefficient of component $i$ in the vapor phase
$\varepsilon$	Composition of the system with maximum order
$\eta$	Non-configurational entropy change
$\omega$	Molar enthalpy change
$\Delta G^E$	Total excess Gibbs free energy
$(PF)_i$	Poynting factor of component $i$

## References

1. Dias, P.; Vilanova, A.; Lopes, T.; Andrade, L.; Mendes, A. Extremely stable bare hematite photoanode for solar water splitting. *Nano Energy* **2016**, *23*, 70–79. [[CrossRef](#)]
2. Tian, H.; Du, L.; Wei, X.; Deng, S.; Wang, W.; Ding, J. Enhanced thermal conductivity of ternary carbonate salt phase change material with Mg particles for solar thermal energy storage. *Appl. Energy* **2017**, *204*, 525–530. [[CrossRef](#)]
3. Islam, M.T.; Huda, N.; Abdullah, A.B.; Saidur, R. A comprehensive review of state-of-the-art concentrating solar power (CSP) technologies: Current status and research trends. *Renew. Sustain. Energy Rev.* **2018**, *91*, 987–1018. [[CrossRef](#)]
4. Ferreira, A.; Kunh, S.S.; Fagnani, K.C.; De Souza, T.A.; Tonezer, C.; Dos Santos, G.R.; Coimbra-Araújo, C.H. Economic overview of the use and production of photovoltaic solar energy in Brazil. *Renew. Sustain. Energy Rev.* **2018**, *81*, 181–191. [[CrossRef](#)]
5. Sun, J.; Liu, Q.; Hong, H. Numerical study of parabolic-trough direct steam generation loop in recirculation mode: Characteristics, performance and general operation strategy. *Energy Convers. Manag.* **2015**, *96*, 287–302. [[CrossRef](#)]

6. Myers, P.D., Jr.; Goswami, D.Y. Thermal energy storage using chloride salts and their eutectics. *Appl. Therm. Eng.* **2016**, *109*, 889–900. [[CrossRef](#)]
7. Aneke, M.; Wang, M. Energy storage technologies and real life applications—A state of the art review. *Appl. Energy* **2016**, *179*, 350–377. [[CrossRef](#)]
8. Liu, M.; Tay, N.S.; Bell, S.; Belusko, M.; Jacob, R.; Will, G.; Saman, W.; Bruno, F. Review on concentrating solar power plants and new developments in high temperature thermal energy storage technologies. *Renew. Sustain. Energy Rev.* **2016**, *53*, 1411–1432. [[CrossRef](#)]
9. Zavoico, A.B. *Solar Power Tower Design Basis Document*; Sandia National Laboratories: Livermore, CA, USA, 2001. [[CrossRef](#)]
10. Badger Energy Corporation. *Design, Handling, Operation and Maintenance Procedures for Hitec Molten Salt*; SAND81-8179; Sandia National Laboratories: Livermore, CA, USA, 1981.
11. Kearney, D.; Kelly, B.; Herrmann, U.; Cable, R.; Pacheco, J.; Mahoney, R.; Price, H.; Blake, D.; Nava, P.; Potrovitza, N. Engineering aspects of a molten salt heat transfer fluid in a trough solar field. *Energy* **2004**, *29*, 861–870. [[CrossRef](#)]
12. Fernández, A.; Ushak, S.; Galleguillos, H.; Perez-Trujillo, F.J. Development of new molten salts with  $\text{LiNO}_3$  and  $\text{Ca}(\text{NO}_3)_2$  for energy storage in CSP plants. *Appl. Energy* **2014**, *119*, 131–140. [[CrossRef](#)]
13. Nunes, V.M.B.; Queirós, C.S.; Lourenço, M.J.V.; Santos, F.J.V.; De Castro, C.N. Molten salts as engineering fluids—A review: Part I. Molten alkali nitrates. *Appl. Energy* **2016**, *11*, 603–611. [[CrossRef](#)]
14. Peng, Q.; Yang, X.; Ding, J.; Wei, X.; Yang, Y. Experimental study and mechanism analysis for high-temperature thermal stability of ternary nitrate salt. *CIESC J.* **2013**, *64*, 1507–1512. [[CrossRef](#)]
15. Ding, J.; Du, L.; Pan, G.; Lu, J.; Wei, X.; Li, J.; Wang, W.; Yan, J. Molecular dynamics simulations of the local structures and thermodynamic properties on molten alkali carbonate  $\text{K}_2\text{CO}_3$ . *Appl. Energy* **2018**, *220*, 536–544. [[CrossRef](#)]
16. Villada, C.; Ding, W.; Bonk, A.; Bauer, T. Engineering molten  $\text{Mg}_2\text{-KCl-NaCl}$  salt for high-temperature thermal energy storage: Review on salt properties and corrosion control strategies. *Sol. Energy Mater. Sol. Cells* **2021**, *232*, 111344. [[CrossRef](#)]
17. Fernández, A.G.; Gomez-Vidal, J.; Oro, E.; Kruiženga, A.; Solé, A.; Cabeza, L.F. Mainstreaming commercial CSP systems: A technology review. *Renew. Energy* **2019**, *140*, 152–176. [[CrossRef](#)]
18. Sau, S.; Tizzoni, A.; Corsaro, N.; Veca, E.; Navas, M.; Martinez-Tarifa, A. Report on protocols for standardized testing procedures and data analysis criteria (Version 1). *Zenodo* **2015**. [[CrossRef](#)]
19. Raade, J.W.; Padowitz, D. Development of Molten Salt Heat Transfer Fluid With Low Melting Point and High Thermal Stability. *J. Sol. Energy Eng.* **2011**, *133*, 031013. [[CrossRef](#)]
20. Xu, X.; Wang, X.; Li, P.; Li, Y.; Hao, Q.; Xiao, B.; Elsentriecy, H.; Gervasio, D. Experimental Test of Properties of  $\text{KCl-Mg}_2$  Eutectic Molten Salt for Heat Transfer and Thermal Storage Fluid in Concentrated Solar Power Systems. *J. Sol. Energy Eng.* **2018**, *140*, 051011. [[CrossRef](#)]
21. Du, L.; Ding, J.; Tian, H.; Wang, W.; Wei, X.; Song, M. Thermal properties and thermal stability of the ternary eutectic salt  $\text{NaCl-Ca}_2\text{-Mg}_2$  used in hightemperature thermal energy storage process. *Appl. Energy* **2017**, *204*, 1225–1230. [[CrossRef](#)]
22. Maksoud, L.; Bauer, T. Experimental investigation of chloride molten salts for thermal energy storage applications. In Proceedings of the 10th International Conference on Molten Salt Chemistry and Technology, Shenyang, China, 10–14 June 2015; pp. 273–280.
23. Mohan, G.; Venkataraman, M.; Gomez-Vidal, J.; Coventry, J. Assessment of a novel ternary eutectic chloride salt for next generation high-temperature sensible heat storage. *Energy Convers. Manag.* **2018**, *167*, 156–164. [[CrossRef](#)]
24. Pelton, A.D.; Chartrand, P. Thermodynamic evaluation and optimization of the  $\text{LiCl-NaCl-KCl-RbCl-CsCl-Mg}_2\text{-Ca}_2$  system using the modified quasi-chemical model. *Metall. Mater. Trans. A* **2001**, *32*, 1361–1383. [[CrossRef](#)]
25. Robelin, C.; Chartrand, P.; Pelton, A.D. Thermodynamic evaluation and optimization of the  $(\text{NaCl}+\text{KCl}+\text{Mg}_2+\text{Ca}_2+\text{Mn}_2+\text{Fe}_2+\text{Co}_2+\text{Ni}_2)$  System. *J. Chem. Thermodyn.* **2004**, *36*, 809–828. [[CrossRef](#)]
26. Robelin, C.; Chartrand, P. Thermodynamic evaluation and optimization of the  $(\text{NaCl}+\text{KCl}+\text{Mg}_2+\text{Ca}_2+\text{ZnCl}_2)$  system. *J. Chem. Thermodyn.* **2011**, *43*, 377–391. [[CrossRef](#)]
27. Foosnaes, T.; Oestvold, T.; Oeye, H.A. Calculation of charge asymmetric additive ternary phase diagrams with and without compound formation. *Acta Chem. Scand. Ser. A Phys. Inorg. Chem.* **1978**, *32*, 973–987. [[CrossRef](#)]
28. Fried, V.; Hameka, H.F.; Blukis, U. *Physical Chemistry*; Macmillan Publishing Co., Inc.: New York, NY, USA, 1977.
29. Bilski, P.; Bobrowicz-Sarga, L.; Czarnecki, P.; Marczak, A.; Wasicki, J. The p–T phase diagram for new ferroelectric bis-thiourea pyridinium bromide. *J. Chem. Thermodyn.* **2013**, *59*, 182–187. [[CrossRef](#)]
30. Nipan, G.D. p–T–x–y phase diagram of the  $\text{Cd-Zn-Te}$  system. *J. Alloy. Compd.* **2004**, *371*, 160–163. [[CrossRef](#)]
31. Smith, J.M.; Van Ness, H.C.; Abbott, M.M. *Introduction to Chemical Engineering Thermodynamics*, 6th ed.; McGraw-Hill Book Co.: New York, NY, USA, 2001.
32. Poling, B.E.; Prausnitz, J.M.; O’Connell, J.P. *The Properties of Gases and Liquids*, 5th ed.; McGraw-Hill Book Co.: New York, NY, USA, 2001.
33. Pelton, A.D.; Blander, M. *Proceedings of the AIME Symposium on Molten Salts and Slags, Nevada, 1984*; Tahoe, L., Ed.; TMS-AIME: Warrendale, PA, USA, 1984; pp. 281–294.
34. Pelton, A.D.; Blander, M. Thermodynamic analysis of ordered liquid solutions by a modified quasichemical approach—Application to silicate salts. *Metall. Trans. B* **1986**, *17*, 805–815. [[CrossRef](#)]
35. Blander, M.; Pelton, A.D. Thermodynamic analysis of binary liquid silicates and prediction of ternary solution properties by modified quasichemical equations. *Geochim. Cosmochim. Acta* **1987**, *51*, 85–95. [[CrossRef](#)]

36. Peng, Q.; Ding, J.; Wei, X.; Yang, J.; Yang, X. The preparation and properties of multi-component molten salts. *Appl. Energy* **2010**, *87*, 2812–2817. [[CrossRef](#)]
37. Li, R.; Gu, W. Calculation of thermodynamic properties of NaCl-KCl system. *Eng. Chem. Metall.* **1989**, *10*, 24–30.
38. Bale, C.W.; Bélisle, E.; Chartrand, P.; Decterov, S.A.; Eriksson, G.; Gheribi, A.; Hack, K.; Jung, I.-H.; Melançon, J.; Pelton, A.D.; et al. Recent Developments in factsage thermochemical software and databases. In *Celebrating the Megascale*; Springer: Cham, Switzerland, 2014; pp. 141–148. [[CrossRef](#)]
39. Egan, J.J.; Bracker, J. Thermodynamic properties of some binary fused chloride mixtures obtained from e.m.f. measurements. *J. Chem. Thermodyn.* **1974**, *6*, 9–16. [[CrossRef](#)]
40. Janz, G.J.; Allen, C.B.; Downey, J.R., Jr.; Tomkins, R.P.T. *Physical Properties Data Compilations Relevant to Energy Storage. 1. Molten Salts: Eutectic Data*; U.S. Government Printing Office: Washington, DC, USA, 1978.
41. Janz, G.J.; Allen, C.B.; Bansal, N.P.; Murphy, R.M.; Tomkins, R.P.T. *Physical Properties Data Compilations Relevant to Energy Storage. 2. Molten Salts: Data on Single and Multi-Component Salt Systems*; U.S. Government Printing Office: Washington, DC, USA, 1981.